

Amyloid precursor protein localises to ependymal cilia in vertebrates and is required for ciliogenesis and brain development in zebrafish

Jasmine Chebli

Institute of Neuroscience and Physiology, Department of Psychiatry and Neurochemistry, The Sahlgrenska Academy, University of Gothenburg

Maryam Rahmati

Institute of Neuroscience and Physiology, Department of Psychiatry and Neurochemistry, The Sahlgrenska Academy, University of Gothenburg

Tammaryn Lashley

Department of Neurodegenerative Disease, UCL Institute of Neurology, Queen Square, London

Brigitta Edeman

Department of Laboratory Medicine, University of Gothenburg

Anders Oldfors

Department of Laboratory Medicine, University of Gothenburg

Henrik Zetterberg

Clinical Neurochemistry Laboratory, Sahlgrenska University Hospital, Mölndal

Alexandra Abramsson (✉ alexandra.abramsson@neuro.gu.se)

Institute of Neuroscience and Physiology, Department of Psychiatry and Neurochemistry, The Sahlgrenska Academy, University of Gothenburg

Research Article

Keywords: Amyloid precursor protein (APP), orthologues, Appa and Appb, APLP1, APLP2, amyloid-beta peptide (A β)

Posted Date: July 8th, 2021

DOI: <https://doi.org/10.21203/rs.3.rs-629681/v1>

License:  This work is licensed under a Creative Commons Attribution 4.0 International License.

[Read Full License](#)

1 **Amyloid precursor protein localises to ependymal cilia in**
2 **vertebrates and is required for ciliogenesis and brain development**
3 **in zebrafish**

4

5 Jasmine Chebli¹, Maryam Rahmati¹, Tammaryn Lashley^{2,3}, Birgitta Edeman⁴, Anders Oldfors⁴,
6 Henrik Zetterberg^{1,3,5,6} and Alexandra Abramsson^{1*}

7

8 ¹*Institute of Neuroscience and Physiology, Department of Psychiatry and Neurochemistry, The*
9 *Sahlgrenska Academy, University of Gothenburg, Gothenburg, Sweden.*

10 ²*Queen Square Brain Bank for Neurological Disorders, Department of Clinical and Movement*
11 *Neurosciences, Queen Square Institute of Neurology, University College London, London, UK.*

12 ³*Department of Neurodegenerative Disease, UCL Institute of Neurology, Queen Square, London, United*
13 *Kingdom.*

14 ⁴*Department of Laboratory Medicine, University of Gothenburg, Gothenburg, Sweden.*

15 ⁵*Clinical Neurochemistry Laboratory, Sahlgrenska University Hospital, Mölndal, Sweden.*

16 ⁶*UK Dementia Research Institute, London, United Kingdom.*

17

18 *Corresponding author: alexandra.abramsson@neuro.gu.se. Institute of Neuroscience and Physiology,
19 Department of Psychiatry and Neurochemistry, The Sahlgrenska Academy, University of Gothenburg,
20 S-41345 Gothenburg, Sweden.

21

22 **Abstract**

23 Amyloid precursor protein (APP) is ubiquitously expressed in human, mice and in zebrafish.
24 In zebrafish, there are two orthologues, Appa and Appb. Interestingly, some cellular processes
25 associated with APP overlap with cilia-mediated functions. Whereas the localization of APP to
26 primary cilia of *in vitro*-cultured cells has been reported, we addressed the presence of APP in
27 motile and in non-motile sensory cilia and its potential implication for ciliogenesis using
28 zebrafish, mouse, and human samples. We report that Appa and Appb are expressed by ciliated
29 cells and become localized at the membrane of cilia in the olfactory epithelium, otic vesicle and

30 in the brain ventricles of zebrafish embryos. App in ependymal cilia persisted in adult zebrafish
31 and was also detected in mouse and human brain. Finally, we found morphologically abnormal
32 ependymal cilia and smaller brain ventricles in *appa*^{-/-}*appb*^{-/-} mutant zebrafish. Our findings
33 demonstrate an evolutionary conserved localisation of APP to cilia and suggest a role of App
34 in ciliogenesis and cilia-related functions.

35

36 **Introduction**

37 Amyloid precursor protein (APP) is a ubiquitously expressed type-1 transmembrane protein
38 that, together with the APP-like protein 1 and -2 (APLP1, APLP2), comprises the *APP* gene
39 family. In addition to their various splice forms, they are all post-translationally modified
40 through proteolytic processing ¹. Although the physiological relevance of the fragments
41 generated is not fully understood, one of these, the amyloid-beta peptide (A β) originating from
42 the transmembrane domain of the APP protein, is the main component of brain amyloid plaques
43 in Alzheimer's disease (AD) ^{1,2}. Beyond its pathological involvement, studies on APP have
44 revealed essential physiological functions including neurogenesis ^{3,4}, neurite outgrowth ^{5,6},
45 adhesion properties ^{6,7}, synapse formation ⁸, and neuronal migration ^{6,9,10}. Nevertheless, the
46 involvement of each APP family member in these processes remains unclear, since redundancy
47 makes it difficult to unravel the contribution of a specific protein ¹¹. Although the molecular
48 mechanisms behind the APP-related processes are yet to be determined, accumulating evidence
49 support that APP orchestrates cellular processes through receptor-like interactions with both
50 inter- and intra-cellular signaling molecules ⁶.

51 The cilium is a highly conserved organelle across species, which contributes to a wide range of
52 cellular processes ¹². Cilia can broadly be categorized into motile and non-motile. Non-motile
53 cilia include primary cilia, which are ubiquitously expressed on most cells as a single short

54 antenna-like structure, and sensory cilia, that are only expressed by specific cells. Primary cilia
55 are enriched in receptors and sites for inter-cell signaling transduction and are notably
56 implicated in cell division, autophagy, midbrain development, memory and learning abilities
57 ¹³. As for the sensory cilia, they are notably found in the otic vesicle as stereocilia and kinocilia.
58 Motile cilia are present on cells involved in fluid movement including the epithelium of the
59 respiratory tract and the ependymal layer of the brain ventricles. Ependymal cells are derived
60 from radial glial cells and when fully differentiated are decorated with tufts of motile cilia
61 anchored with roots at the apical cellular membrane ^{12,14}. The coordinated periodic beating of
62 the cilia participate in the generation of cerebrospinal fluid (CSF) flow within ventricle cavities
63 ¹⁵. Circulation of CSF is believed to facilitate transfer of signaling molecules and removal of
64 metabolic waste products to prevent accumulation of neurotoxic residues in the brain
65 parenchyma ¹⁶⁻¹⁸.

66 There are several findings supporting a connection between APP and cilia. First, part of the
67 wide range of cilia-mediated functions overlap with processes linked to APP, *e.g.*, cognitive
68 impairment ¹⁹, differentiation of neurons ²⁰, formation of corpus callosum ^{19,21}, neuronal
69 migration ²²⁻²⁴ and sensing of guidance molecules ²⁵. Second, overexpression of APP impairs
70 primary cilia both in a mouse AD model and in individuals with Down syndrome, harboring
71 three copies of *APP* ^{26,27}. The latter is also associated with decreased CSF flow and
72 accumulation of CSF (hydrocephalus), two phenotypes commonly associated with defects in
73 motile cilia ²⁸. Finally, APP has been shown to localize to primary cilia *in vitro* and A β exposure
74 results in reduced cilia length ²⁹. Taken together, these findings warrant further investigations
75 of the role of APP in both motile and non-motile cilia.

76 In the present study, we address the presence of APP in motile and non-motile (sensory) cilia
77 and its possible functions using zebrafish, mouse and human samples. We found that the
78 zebrafish App homologues are expressed by ciliated cells and become localized at the

79 membrane of cilia in the otic vesicle, the nasal epithelium, and the brain ventricles of zebrafish
80 embryos. The presence of App in ependymal cilia persisted in adult zebrafish and was also
81 detected in the ependymal cells of mouse and human brains. In addition, we show that zebrafish
82 embryos with mutations in both *app* paralogues (*appa*^{-/-}*appb*^{-/-}) have morphologically abnormal
83 ependymal cilia and smaller brain ventricles compared with wild-type siblings.

84

85

86 Results

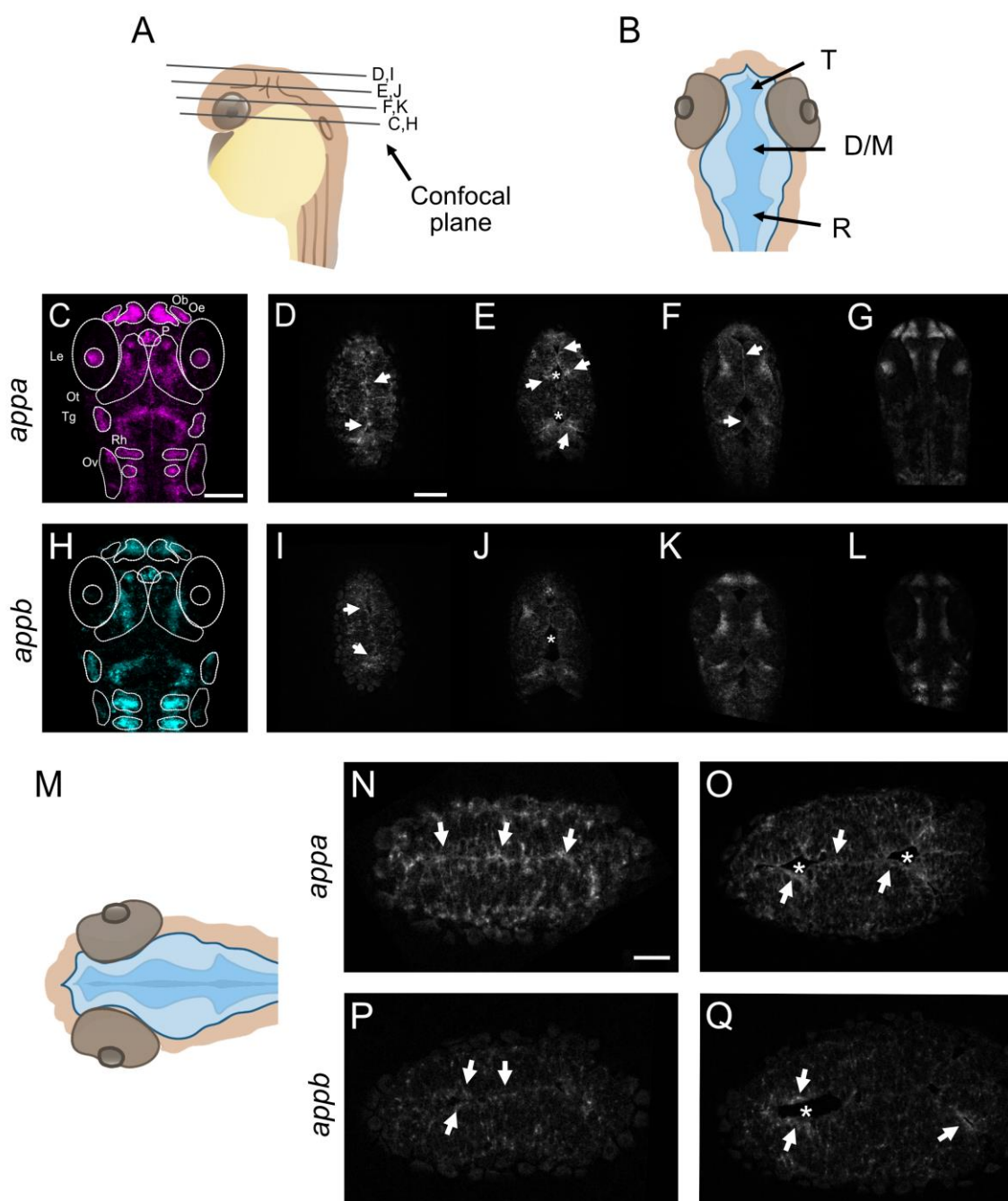
87 *Appa and appb mRNA expression patterns at the brain ventricular limits*

88 The zebrafish *app* genes, *appa* and *appb*, are expressed in the CNS, and have both distinct and
89 shared expression patterns^{7,30}. Due to the lack of specific antibodies, we used fluorescent whole
90 mount *in situ* hybridization to increase the cellular resolution of *appa* and *appb* mRNA
91 expression in areas with motile cilia on 30 hpf wild-type larvae zebrafish (**Figure 1**). Consistent
92 with previous studies, we observed *appa* mRNA expression in the lens, the olfactory bulb and
93 epithelium, in the trigeminal ganglia and in the otic vesicle. (**Figure 1C**). Similarly, the *appb*
94 mRNA expression signal corroborated previous data on *appb* mRNA expression³⁰ in the
95 olfactory and otic vesicle epithelia (**Figure 1H**).

96 In addition, both *appa* (**Figures 1C-G and high magnification Figures 1N,O**) and *appb*
97 (**Figures 1H-L, P,Q**) mRNA signals labelled cells lining the diencephalic ventricle both in the
98 dorsal and ventral areas. Negative controls did not show any specific signal (**Supplementary**
99 **file 1**). Together, these results show expression of *appa* and *appb* in areas with ciliated cells,
100 including cells lining brain ventricles, otic vesicle and olfactory organ, thus suggesting a
101 possible role of App in cilia formation and function.

102

Figure 1. Expression of *appa* and *appb* mRNA in zebrafish larvae



103

104

105 ***App protein is localized to cilia of the olfactory sensory neurons and otic vesicle in zebrafish***
106 ***larvae***

107 The expression of both *appa* and *appb* in ciliated cells made us ask if the proteins become
108 distributed out to the cilia. The zebrafish olfactory epithelium and the otic vesicle comprise
109 ciliated cells and are regions where both *appa* and *appb* mRNAs are expressed. To address if
110 Appa and Appb become localized to these cilia, we performed immunofluorescent staining on
111 zebrafish larvae.

112 ***Olfactory sensory neuron cilia***

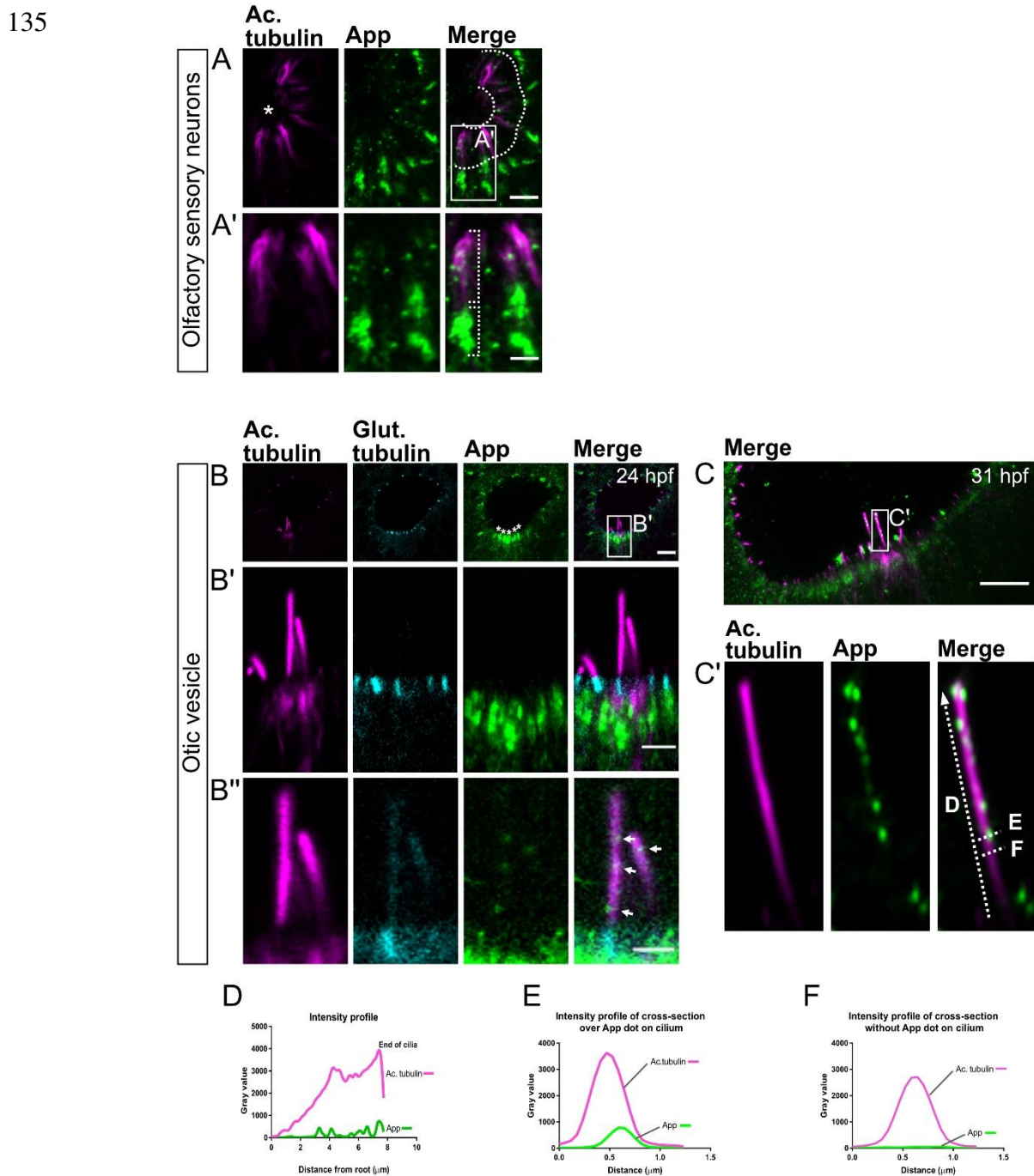
113 We used the Y188 antibody, binding to a conserved epitope in the C-terminal end of human,
114 mouse, and zebrafish App (***Figure 6C***), in combination with the anti-acetylated tubulin
115 antibody, labelling microtubule structures of cilia. Immunofluorescent co-labelling detected a
116 punctate App signal in the heavily ciliated olfactory epithelium area at 30 hpf (***Figure 2A***).
117 However, while the resolution of the images did not allow distinction between each cilium, App
118 signal seemed to localize to most of them. In addition to the cilium, App expression was also
119 found at the base of these motile cilia (***Figure 2A'***).

120 ***Otic vesicle cilia***

121 Similar to the olfactory neurons, high accumulation of App was noted at the base of the cilia in
122 the otic vesicle. In zebrafish, hair cells of the otic vesicle have two types of cilia, a long single
123 kinocilium and a bundle of shorter stereocilia³¹. The immunofluorescent staining revealed App
124 expression in both types of cilia at early time points in the larvae development (***Figures 2B-C***).
125 Staining of 24 hpf larvae with glutamylated tubulin, highlighting the cilia basal body, clearly
126 showed an App signal within the hair cells and close to the basal body (***Figures 2B, B',B''***).
127 App expression became more distinct at 30 hpf (***Figure 2C***). Plots of the intensity profile of
128 App (green) and acetylated tubulin (magenta) showed a punctate distribution of App throughout

129 the kinocilium (**Figure 2D**), which supports that App localizes to the cilium membrane (**Figure**
 130 **2E**). No signal was detected in the intensity profile in the absence of App puncta (**Figure 2F**),
 131 and the negative control (absence of primary antibody) was negative (*Supplementary file 2*).
 132 Together, these data show expression of App in cilia and ciliated cells of the otic vesicle and
 133 olfactory bulb and indicate that App is located at the cilium membrane.

134
Figure 2. App protein is localized to non-primary cilia in zebrafish larvae



136 ***App localizes to cilia decorating the brain ventricle surface of zebrafish***

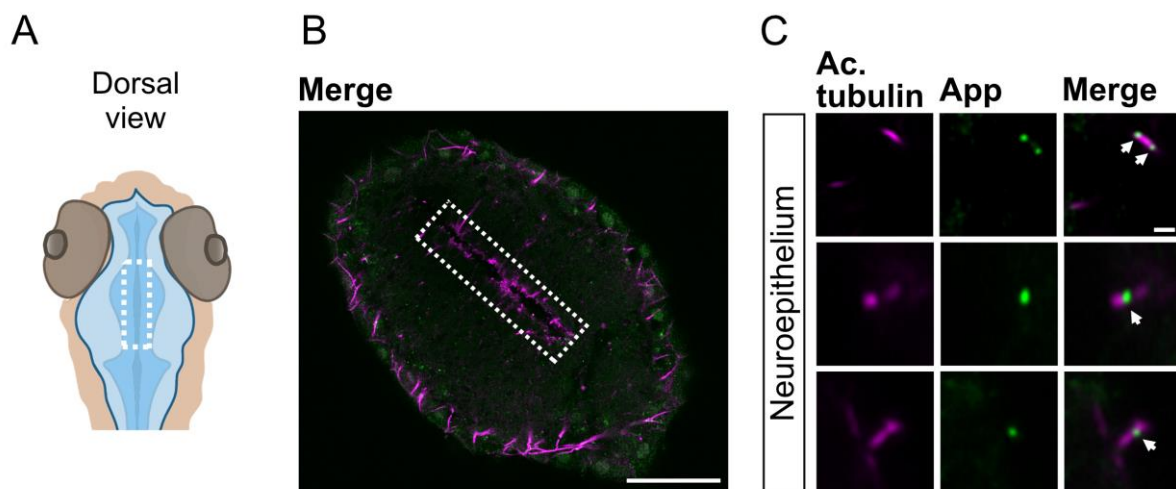
137 As APP was previously shown to be expressed by the ependymal cells in rodents and in humans
138³²⁻³⁴, we explored App expression by ependymal cells and App localization at their cilia in
139 larvae and adult zebrafish (**Figure 3**). At 30 hpf, the brain ventricles are inflated and the
140 differentiation of motile cilia in the most ventral and dorsal regions have just started but do not
141 yet contribute to directional CSF flow ³⁵. This facilitates whole-mount imaging and
142 measurement of single cilium. Using the same combination of antibodies (anti-APP (Y188) and
143 anti-acetylated tubulin) as above, we could detect App-positive puncta along the acetylated
144 tubulin signal in most cilia (**Figures 3B,C**). To address if App localization to cilia is maintained
145 into adulthood, we performed immunofluorescent staining on coronal sections of adult
146 zebrafish brains using antibodies detecting App (Y188) and acetylated tubulin to label cilia.
147 Our results showed that consistent to larvae, App was distributed to ependymal cilia in the adult
148 brain. In contrast to larvae, ependymal cells in adult individuals were covered with multiple
149 motile cilia. Cryosections of adult zebrafish brain revealed dense cilia tufts with App-positive
150 staining at the apical side of the ependymal cells (**Figures 3E,F**). Furthermore, App was also
151 expressed by ependymal cells, similarly to what has previously been described in rodents and
152 humans (**Figure 3F**). Negative controls did not show any cilia-specific staining
153 (**Supplementary file 3**).

154

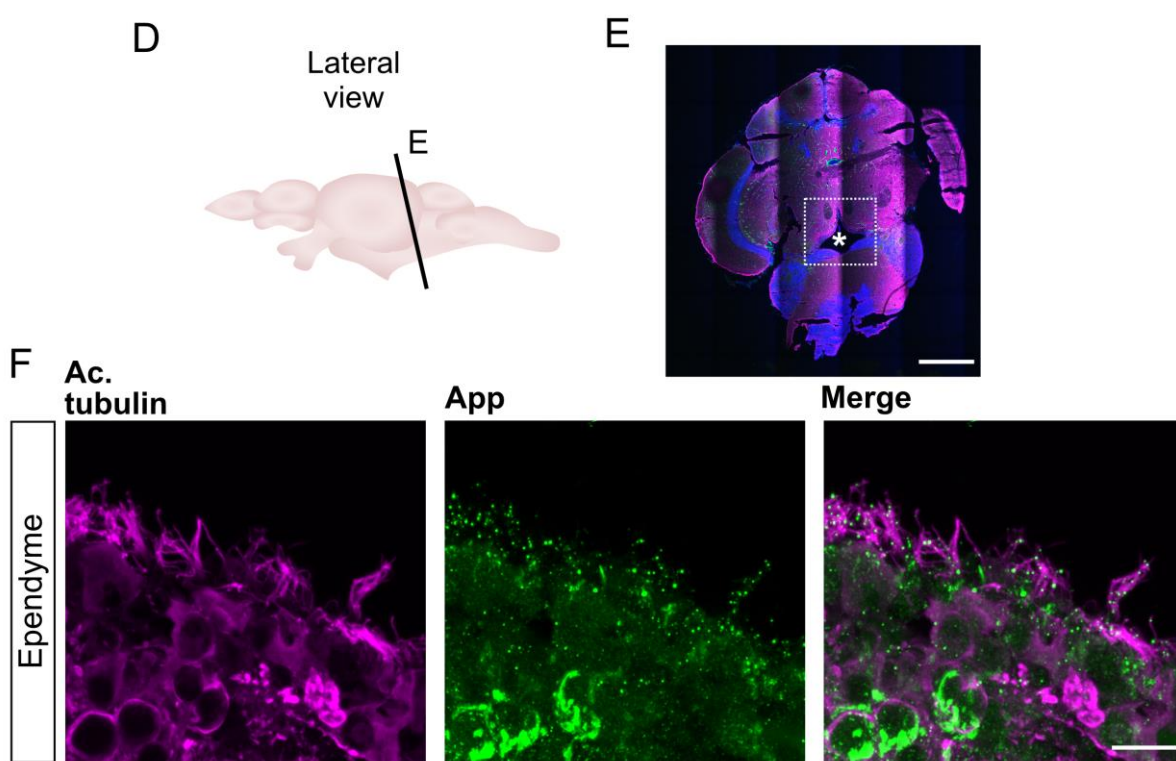
155

Figure 3. App is localized to the cilia membrane of neuroepithelium and ependyme in larvae and adult zebrafish

Zebrafish larvae



Zebrafish adult



156

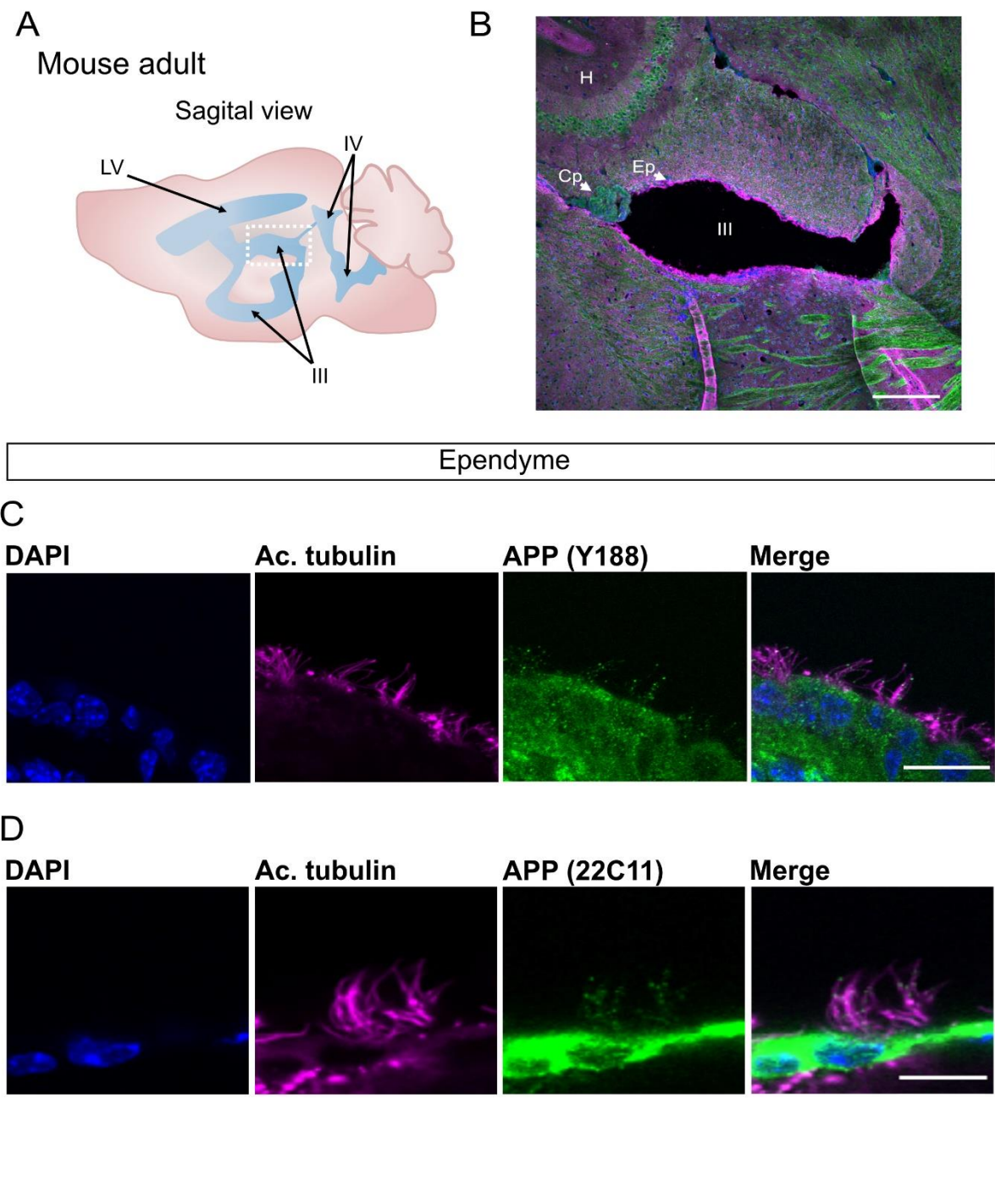
157

158 ***Conserved localization of APP in ependymal cilia in mouse and human brains***

159 APP is also localized to ependymal cilia in mice and humans. We performed immunostaining
160 on mouse brain sections using two antibodies directed to APP, Y188 binding to the C-terminal
161 intra-cellular domain and 22C11 detecting the E1 domain of the N-terminal region (**Figure 6C**),
162 together with anti-acetylated tubulin. The ependymal motile cilia were easily localized in the
163 third ventricle of the brain sagittal section (**Figures 4A,B**). Congruent with our results on adult
164 zebrafish brains, we detected strong APP expression with both antibodies throughout the
165 ependymal cells layer and punctate APP staining (Y188 see **Figure 4C** and 22C11 see **Figure**
166 **4D**) overlapping with acetylated tubulin-positive cilia. Interestingly, APP expression by the
167 choroid plexus cells was detectable (**Figure 4B**). Negative control for primary antibodies was
168 performed and showed no or weak signal (**Supplementary file 4**).

169

Figure 4. APP is localized to the ependymal cilia in adult mouse



173 In the human brain, acetylated tubulin staining allowed separation of cellular layers of the
174 caudate nucleus and identification of acetylated tubulin-positive cilia of the ependymal cell
175 layer lining the lateral ventricle (***Figures 5A,B,D***). However, while many ependymal cells had
176 intact cilia, many were found broken and dislocated from their cell (***Supplementary file 5***).

177 To address the presence of APP in ependymal cilia, brain serial sections of the caudate nucleus
178 were incubated with horseradish peroxidase (HRP)-conjugated Y188 or A8717 antibodies, both
179 recognizing the C-terminal domain of APP. Similarly to our results obtained in mouse and
180 zebrafish brains, brightfield images confirmed strong APP expression in the ependymal cells
181 and, upon higher magnification, in ependymal cilia (***Figures 5C,E , Supplementary file 5***). In
182 contrast to zebrafish and mouse, APP in human ependymal cilia was evenly distributed and was
183 not detected as puncta.

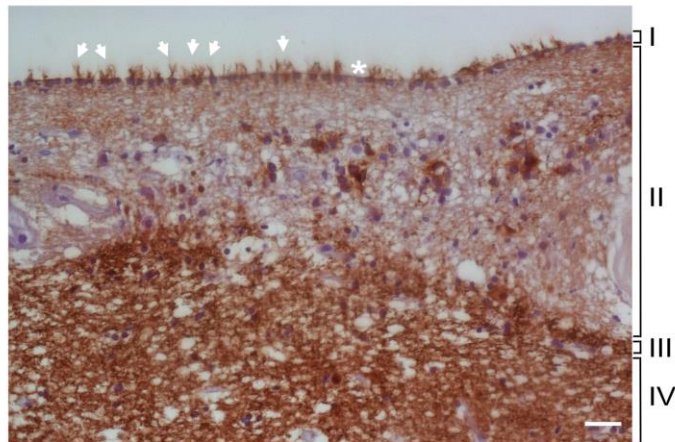
184 In summary, these results show that the expression of APP in the ependymal cells and their cilia
185 are conserved between species as far apart as zebrafish, mice, and humans.

186

Figure 5. APP is localized to human brain ependymal cilia

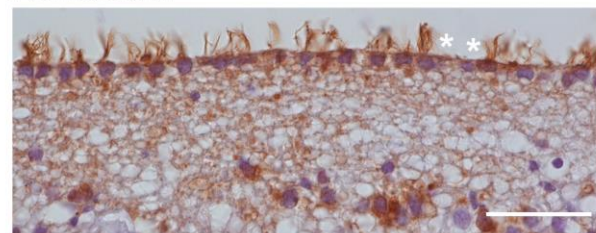
A

Ac. tubulin



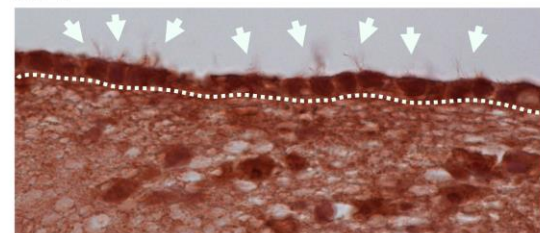
B

Ac. tubulin



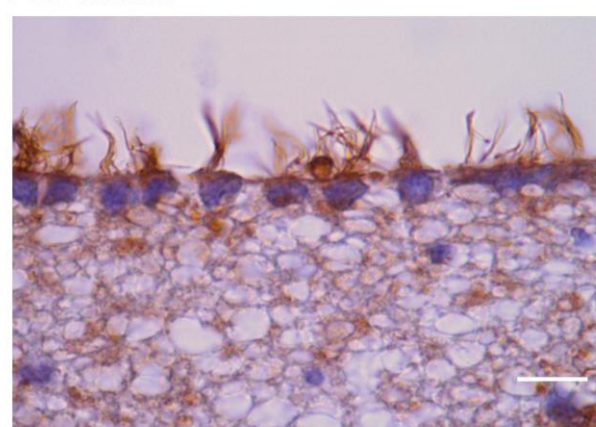
C

APP



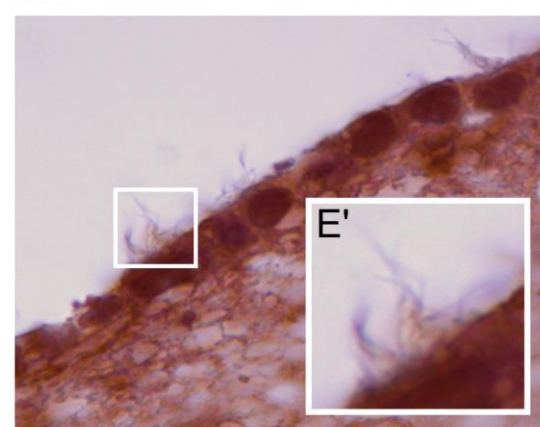
D

Ac. tubulin



E

APP

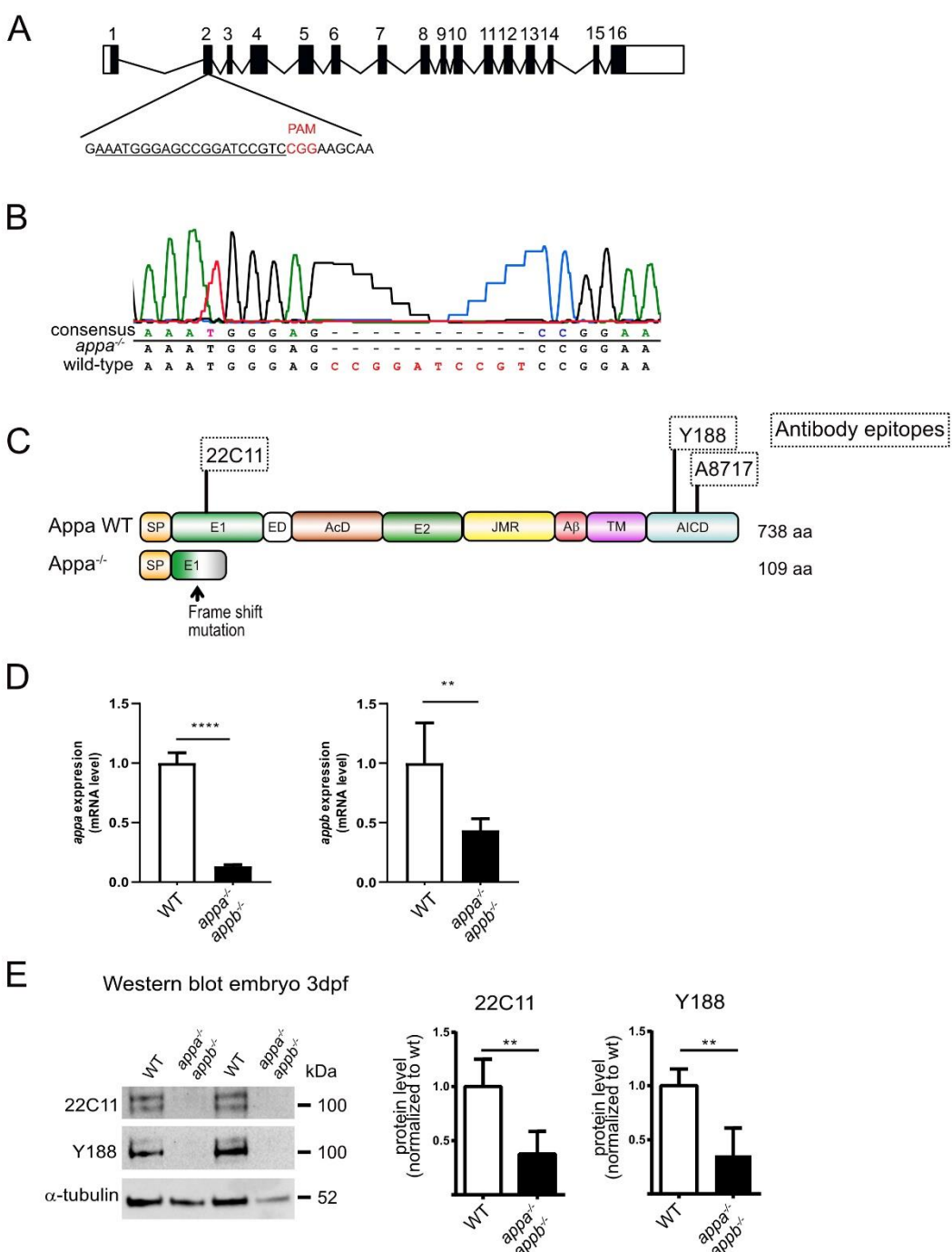


189 ***Generation of appa and app double mutant zebrafish***

190 In contrast to humans and mice, zebrafish have two *APP* orthologues, *appa* and *appb* (together
191 designated *app*). Zebrafish with mutated *appb* gene was generated and described by our lab
192 previously⁷. However, to investigate the requirement of both App proteins in ciliogenesis, we
193 used the CRISPR/Cas9 method to generate mutations in the zebrafish *appa* gene (**Figure 6A**).
194 A mutation was identified in exon 2 (**Figure 6A**), and Sanger sequencing confirmed a frame
195 shift mutation of 10 nucleotides (**Figure 6B**). The mutation resulted in a premature stop codon
196 that is predicted to give rise to a protein truncation at amino acid 109 (**Figure 6C**). The *appa*
197 mutant allele was outcrossed into the AB background until generation F4 and then bred with
198 the *appb*^{-/-} to generate the double mutant *appa*^{-/-}*appb*^{-/-} zebrafish line. The *app* mutant zebrafish
199 were healthy and fertile and did not show any gross morphological phenotypes. qPCR analysis
200 of genes expression showed very low *appa* and *appb* mRNA levels in the double mutant fish
201 line (**Figure 6D**). Western blot analysis using the Y188 and 22C11 antibodies with epitopes in
202 the intracellular and extracellular domain, respectively, showed decreased protein levels in *app*
203 double-mutant larvae (**Figure 6E and Supplementary file 6**). Both antibodies are likely cross-
204 reacting with Aplp2 since the epitope sequences are highly similar. These data show that the
205 introduced mutation in *appa* resulted in a significant decrease of both transcription and
206 translation of the Appa protein indicating that the mutation give rise to a loss-of-function
207 mutation.

208

Figure 6. Generation of *appa*^{-/-} zebrafish



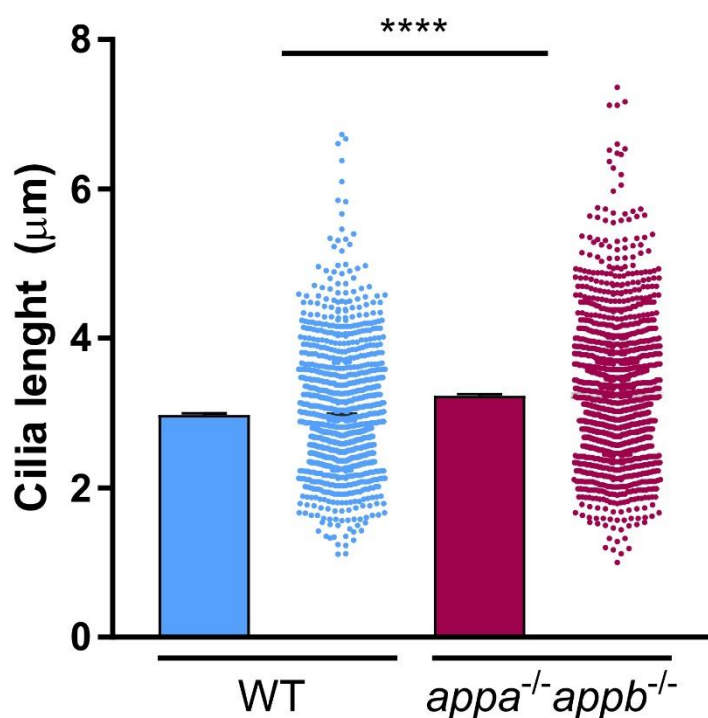
209

210

211 **Longer brain ventricle cilia in *appa*^{-/-}*appb*^{-/-} larvae**

212 The conserved distribution of APP in brain ventricle cilia prompted us to address the
213 requirement of App during ciliogenesis. We measured the length of cilia in the midbrain
214 ventricle detected by acetylated tubulin immunostaining signal in both *appa*^{-/-}*appb*^{-/-} double
215 mutants and wildtype larvae at 30 hpf. At this stage, the cilia delineating the dorsal and ventral
216 parts of the diencephalic ventricles are not yet motile³⁵. A 3D-region of interest (ROI) was used
217 to measure cilia length. The ROI was established from the dorsal part of the midbrain ventricle
218 to the ventricular space at a depth of around 25 µm. To our surprise, we found that the
219 ependymal cilia in the ROI were significantly longer in *appa*^{-/-}*appb*^{-/-} mutants compared with
220 wild-type larvae (**Figure 7**), which was confirmed by frequency distribution (**Supplementary**
221 **file 7**).

Figure 7. Longer cilia of brain ventricle neuroepithelium in *appa*^{-/-}*appb*^{-/-} larvae zebrafish



222

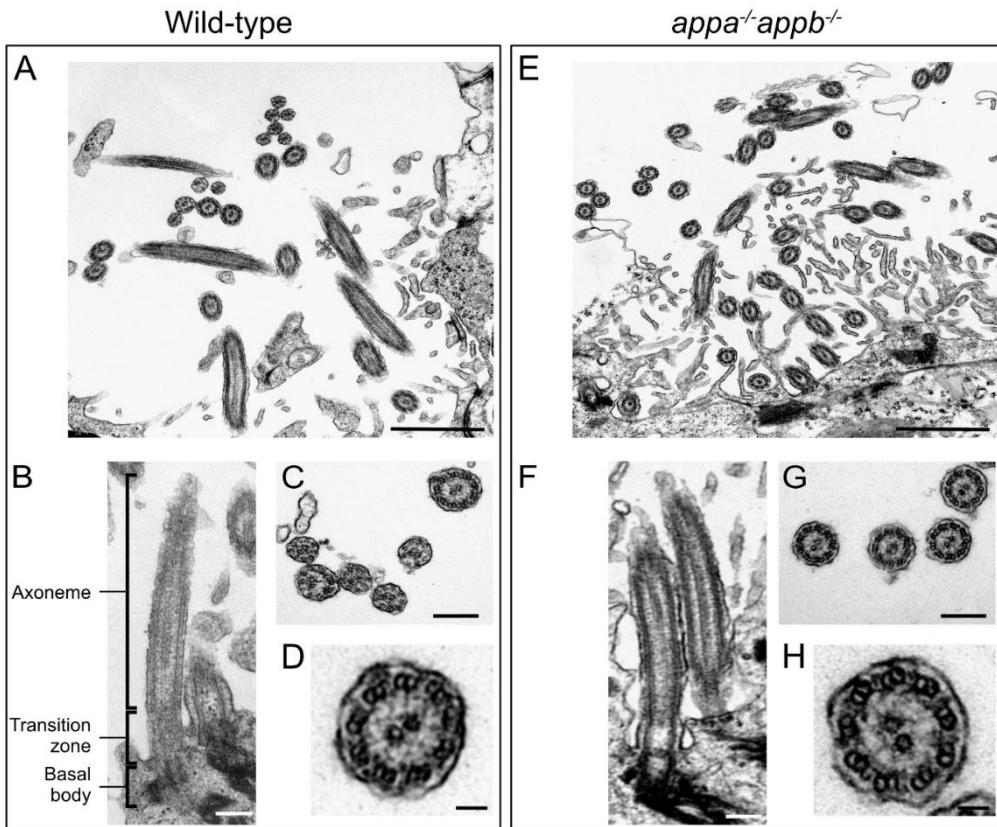
223

224 ***Integrity of ependymal cilia axoneme and microtubule doublets in motile brain ependymal***
225 ***cilia in appa^{-/-}appb^{-/-} mutant adult zebrafish***

226 Emerging from the basal body is the axoneme, which forms the core of the cilium. First
227 described in the early 1950s with electron microscopy, axonemes are composed of nine
228 microtubule doublets at the periphery (9+0)³⁶. In some cilia, an additional central doublet is
229 expressed (9+2), allowing cilia to generate and regulate movement^{37,38}. This central
230 microtubule doublet is found in motile ependymal cilia (9+2). To better characterize the ciliary
231 ultrastructure of App-deficient zebrafish, we performed transmission electron microscopy
232 (TEM) analysis of ependymal cells in adult zebrafish brains. TEM revealed a normal (9 + 2)
233 axoneme in the cross-sections of ependymal cilia of WT (n=3) brain ventricle (**Figures 8A–D**).
234 In *appa^{-/-}appb^{-/-}* zebrafish (n=4), ependymal cilia showed normal (9+2) axonemes (**Figures 8E–**
235 **H**).

236

237 **Figure 8. Structural integrity of ependymal cilia in WT and *appa^{-/-}appb^{-/-}* zebrafish**

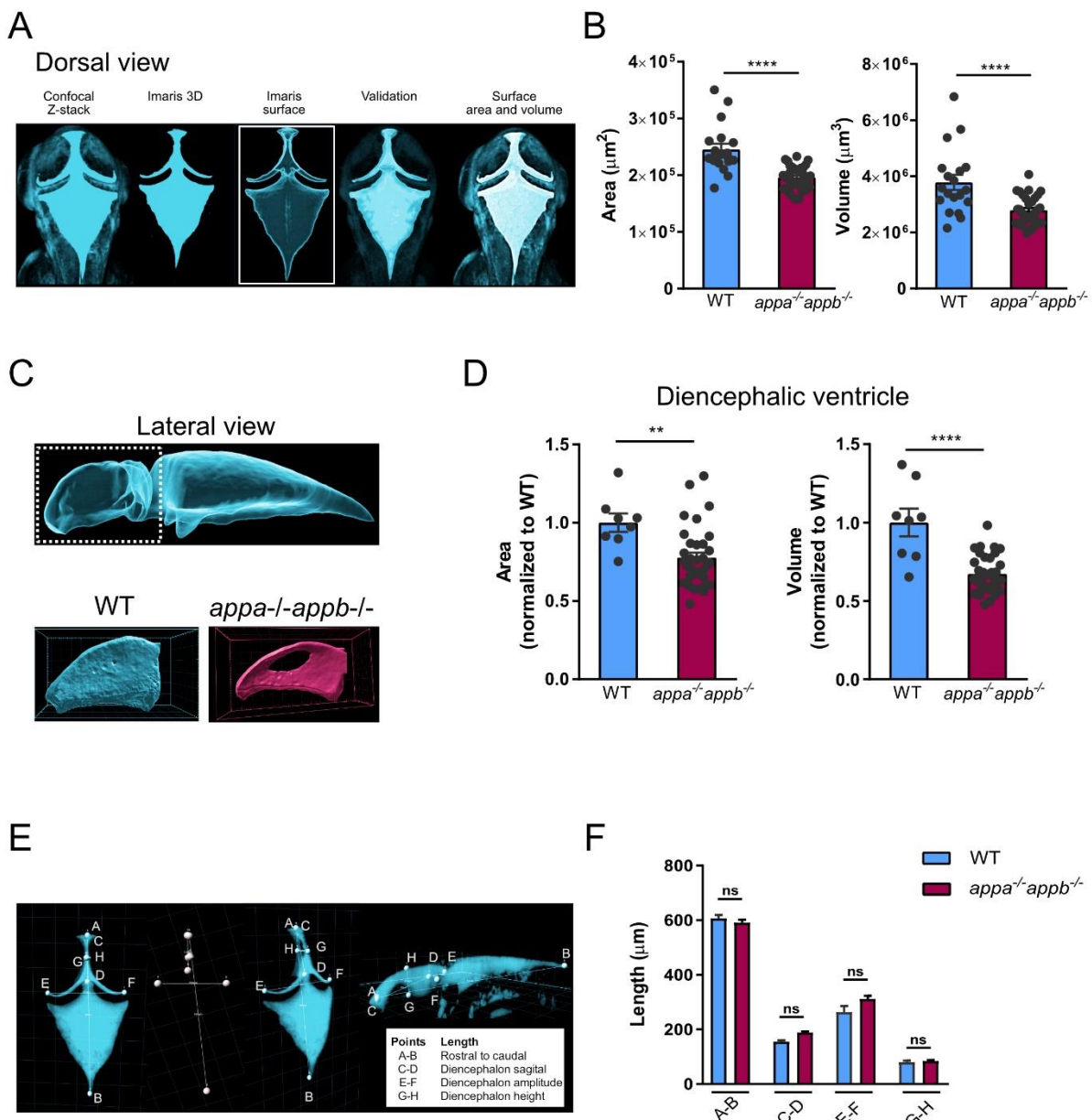


239 ***The appa^{-/-}appb^{-/-} double mutants exhibit smaller diencephalic ventricle***

240 We then went on to address if defects in ependymal cilia affect brain ventricle formation. We
241 analysed brain ventricle volume and area in 2dpf larvae (**Figure 9A**) and found significant
242 reductions in both area and volume of the ventricular space in *appa^{-/-}appb^{-/-}* compared with
243 wild-type (**Figure 9B**). These reductions were also observed when only the diencephalic
244 ventricle was analysed (**Figure 9C**) and compared between both genotypes (**Figure 9D**). The
245 gross morphology was next determined by measuring the length between specific points and
246 areas of the ventricles: rostral to caudal, diencephalon ventricle sagittal length, amplitude and
247 height (**Figure 9E**). However, no significant change was detected compared with wildtype
248 larvae (**Figure 9F**). These results show that while the overall brain morphology of App mutants
249 is maintained, their ventricles are smaller.

250

Figure 9. *appa^{-/-}appb^{-/-}* larvae zebrafish exhibit smaller brain ventricles



251

252

253 **Cilia targeting motifs in App**

254 Many proteins distributed to the cilium carry one or more cilia targeting sequences (CTS). The
255 most common and well-studied are the VxP and AxxxQ motifs, both of which the requirement
256 has been shown in transmembrane proteins including opsins³⁹⁻⁴¹ and somatostatin receptor 3
257 (SSTR3)^{42,43}. The presence of App in cilia therefore made us investigate the presence of these
258 motifs in App. Interestingly, we found several different CTS motifs with most localized to the
259 mid- and C-terminal domain of the App protein (*Supplementary file 8*). Furthermore, most of
260 these are in conserved regions and are thus shared between zebrafish, mouse and human
261 (*Supplementary file 8*).

262

263

264 **Discussion**

265 In this study, we show that App localizes to several different non-motile and motile cilia in
266 zebrafish larvae including the stereo- and kinocilia of the otic vesicle, motile cilia of olfactory
267 sensory neurons in the olfactory epithelium and cilia of the ependymal cells lining the brain
268 ventricles. We also show an evolutionary conserved localization of APP to cilia of the
269 ependymal cells lining the brain ventricles of adult zebrafish, mice and humans. As these results
270 indicated a possible function of APP in ciliogenesis or cilia function, we used zebrafish lacking
271 the two APP orthologues, Appa and Appb, and found longer ependymal cilia and smaller brain
272 ventricles in larvae zebrafish. Thus, our results suggest that APP not only is distributed to cilia
273 but also seems to have an important function in ciliogenesis and brain development.

274 We used different antibodies to confirm the localization of App to the cilia. The punctate
275 localisation of APP indicates that the protein is randomly distributed within the cilium similar
276 to other membrane receptors such as SSTR3 and Smoothened (Smo)^{44,45}. The distribution of

277 APP within the plasma membrane varies between cell types, nonetheless a recent study
278 suggested that APP clusters form groups of proteins within the plasma membrane⁴⁶. The
279 similarity with the punctate pattern found here suggests that App may form clusters within the
280 cilium, at least in zebrafish and mice. In contrast, we observed a continuous rather than punctate
281 distribution of APP in human ependymal cilia. Whether the observed differences are due to
282 sample preparation or variations in APP distribution between species remains to be addressed.
283 Moreover, the accumulation of App at the root of the basal body, as observed in the olfactory
284 sensory neurons and otic vesicle cilia in larvae zebrafish, correlates with the findings reported
285 by Yang and Li on APP enrichment along ciliary rootlets⁴⁷.

286

287 The presence of APP within cilia raises the question of how APP is targeted to the cilium. The
288 cilium membrane is continuous with the plasma membrane, yet it possesses a specific and
289 conserved composition of proteins and lipids. This specification is considered to be established
290 through an active transport of ciliary membrane proteins⁴⁸ that at least partly depends on
291 specific ciliary transport sequences (CTSs) within the proteins⁴⁹. The presence of several such
292 CTSs and their conservation between zebrafish, mice and human supports a motif-based
293 transport of APP to cilia (*Supplementary file 8*). It will therefore be very interesting to address
294 the extent to which these motifs are required for accumulation of APP at the root of the basal
295 body and later distribution of APP out to the cilium.

296

297 APP expression by the ependymal cells was first reported in rodents and humans in the late
298 1980s and early 1990s^{32,33,50,51}. In line with these findings, our results not only confirm the
299 expression of App in adult zebrafish ependymal cells, but in addition, show that APP localizes
300 to ependymal motile cilia in vertebrates as far apart as zebrafish, mice, and humans. Our finding

301 that loss of App results in morphologically abnormal ependymal cilia suggests a role of App in
302 ciliogenesis. However, the *appa*^{-/-}*appb*^{-/-} mutants gave rise to fertile adults without major
303 phenotypic changes associated with cilia defects, such as curved body and hydrocephalus⁵²⁻⁵⁵.
304 In line with our findings, Olstad *et al.* recently reported that such phenotypes mainly associate
305 with primary cilia defects, while changes in motile cilia were more likely to result in ventricle
306 duct occlusion⁵⁶. During early development, movement of cilia is a major factor maintaining
307 CSF flow within ventricles. Consequently, the cilia-driven flow is crucial to form and maintain
308 a proper brain ventricular system, as zebrafish, clawed frog and mouse ciliary mutants display
309 ventricular defects⁵⁶. It is thus likely that the defective ventricle expansion observed in the
310 *appa*^{-/-}*appb*^{-/-} mutant larvae may result from changes in of motile cilia. Although we did not
311 observe a lack of diffusion between ventricles indicating duct occlusion, our data suggest that
312 App may be required in motile cilia to promote flow of CSF needed for ventricle formation
313 during early development⁵⁶. It will thus be interesting to examine the extent to which cilia
314 movement and CSF flow change when altering App levels and at later developmental stages.

315

316 Our findings raise several questions regarding the role of APP in cilia and to which level cellular
317 processes associated with APP may be mediated through cilia. For example, the multi-ciliated
318 ependymal cell layer covering the brain ventricles is important for neurogenesis, both by
319 regulating the number of neural stem cells in the neurogenic niches of the subventricular zone
320⁵¹ and by facilitating the migration of new-born neuronal cells through cilia-regulated fluid
321 dynamics⁵⁷. Interestingly, APP is also reported to regulate neurogenesis⁵⁸⁻⁶⁰ and to promote
322 neuronal migration⁹. Our understanding of APP-mediated processes continues to increase, but
323 the mechanisms by which these processes are orchestrated are yet not fully understood.
324 Therefore, the obvious overlap between functions mediated by ependymal cells and APP makes

325 it tempting to speculate that APP might be important or at least partly required in ependymal
326 cells to mediate cell migration and proliferation.

327

328 The length of cilia can be modified both by changes in the structural proteins involved in
329 microtubule assembly but also depends on the cell proliferation and differentiation status, where
330 proliferating cells generally have shorter cilia than growth arrested cells. As an example,
331 modulation of several cell cycle-related kinases could alter ciliary length⁶¹. This is true for
332 primary cilia but to what extent this is valid for other types of cilia is not yet described. The
333 mechanisms by which App contributes to regulate cilia length is beyond the scope of the present
334 study but could potentially involve its role in cell differentiation⁶.

335 It is intriguing to think of APP in the cilium as a receptor that senses signalling molecules and
336 metabolites transported through the ventricles by CSF. The hypothesis of APP acting as a
337 receptor is supported by its similarities with type I membrane receptors and by the fact that the
338 list of potential APP ligands continues to grow (review by⁶). Therefore, it is tempting to
339 speculate that APP localized on the cilia interacts with CSF-circulating ligands, *e.g.*, Aβ
340 peptides, growth factors, and hormones^{6,62}, to mediate CSF-derived signalling.

341

342 Beyond the impact of App on ciliogenesis during development, it is intriguing to speculate on
343 the long-term effects of impaired near-wall CSF propulsion. This movement is thought to play
344 an important role in removal of waste products from the brain parenchyma⁶³. Thus, it is likely
345 that subtle changes in the coordinated beating of cilia may contribute to altered regional CSF
346 flow that impairs clearance and hence contributes to a slow build-up of waste products over
347 time. In support are findings that individuals with Down syndrome, expressing approximately
348 50% higher levels of APP, have changed CSF flow in the lateral ventricles⁶⁴. Although the

349 morphology of ependymal cilia of DS brains are unknown, *in vitro* cell cultures show decreased
350 primary cilia length²⁶. Investigations addressing cilia morphology and function in the adult
351 zebrafish brain lacking App are ongoing in our lab; however, it will be equally important to
352 perform these experiments in *app*-knockout mice, as well as in mice overexpressing APP,
353 which results in altered post-translational processing of the protein.

354

355 The presence of APP in ependymal cells and their cilia also raises the question regarding their
356 contribution to APP-derived fragments found in CSF. As at least some secretases needed for
357 APP processing are present in cilia⁶⁵, it is likely that the fragments detected in CSF not only
358 originates from the brain parenchyma but also from APP being processed within the ependymal
359 cells and the protruding cilia. The release of APP from ependymal cells could be mediated
360 through the release of extracellular cleavage products or by budding extracellular vesicles and
361 ectosomes. The latter process was in a recent study described as a common mechanism by
362 which proteins are cleared from cilia instead of recycling by retrograde transport⁶⁶. APP-
363 containing vesicles are released into the CSF⁶⁷ and in a recent report, such microvesicles were
364 found to have lower levels of APP in AD patients compared to healthy individuals⁶⁸. The
365 impact of ependymal integrity and the contribution of cilia-mediated APP release need further
366 studies but could potentially contribute to our interpretation of biomarkers used to assess
367 disease progression. Interestingly, a well-established feature of normal pressure hydrocephalus,
368 where ciliary function is impaired⁶⁹, is decreased CSF levels of soluble APP and Aβ, which
369 are restored upon successful shunt treatment of the condition⁷⁰⁻⁷².

370

371 While others have shown that APP and its processing machinery are expressed in the olfactory
372 epithelium and bulb in cultured mouse cells⁷³, we here report App localization also to the

373 olfactory cilia in larvae zebrafish. Motile cilia of the olfactory sensory neurons (OSNs) in
374 zebrafish are essential to generate liquid flow in the nose pit to detect odorant molecules⁷⁴. In
375 zebrafish, the olfactory epithelium can be divided into three categories of OSN, *i.e.*, ciliated,
376 microvillus and crypt OSNs^{75,76}. Each OSN expresses distinct classes of receptors and sensing
377 molecules and has a specific axonal pathway from the olfactory bulb leading towards higher
378 olfactory centres in either the telencephalon or the optic tectum. If APP is present in cilia of all
379 OSN or only a subset, needs to be confirmed. However, the presence of APP in the olfactory
380 cilia could potentially give clues on corresponding pathways and insights into the mechanisms
381 resulting in olfactory deficiencies in AD mouse models and neurodegenerative disease⁷⁷.

382 Hearing is a major sensory input in vertebrates, which is known to decrease with aging.
383 Although the relationship between APP and hearing is less studied than many other areas, there
384 are a few reports pointing to the loss of hearing associated with APP or its cleavage product A β
385⁷⁸⁻⁸⁰. Our data, showing the presence of App in cilia mediating hearing, open up the possibility
386 that nervous system-related changes in hearing may not only be due to defects in the brain
387 regions receiving input from the auditory organ but also due to direct effects on the cilia.
388 However, the function of App in the auditory system needs further investigation.

389

390 Altogether, our data show the presence of App in motile and non-motile cilia of the otic vesicle,
391 olfactory pit and ependymal cells lining the brain ventricles. We also report a conserved
392 distribution, at least in the ependymal cilia, across vertebrates and that App is required for
393 proper ciliogenesis and brain ventricle formation. The evolutionary conserved CTSs of APP
394 and its expression throughout development and aging suggest a central role of APP within the
395 ependyme. Further studies are required to fully understand the impact of App in cilia in our
396 olfactory and auditory organs and to which extent defects in ependymal cell integrity and
397 ciliation contribute to APP-related developmental processes and disease progression.

398 **Methods**

399 ***Animal care and ethics statement***

400 The zebrafish (*Danio rerio*) facilities and maintenance were approved and follow the guidelines
401 of the Swedish National Board for Laboratory Animals. This study was approved by the Animal
402 Ethical Committee at the University of Gothenburg. All procedures for the experiments were
403 performed in accordance with the animal welfare guidelines of the Swedish National Board for
404 Laboratory Animals and followed the recommendations in the ARRIVE guidelines ⁸¹.
405 Zebrafish were maintained in Aquatic Housing Systems (Aquaneering, San Diego, CA) at 28.5
406 °C, under a 14:10 hour (h) light:dark cycle at the Institute of Neuroscience and Physiology,
407 University of Gothenburg. Fish were fed twice daily a diet of live-hatched brine shrimps and
408 Gemma fish food (Skretting, Amersfoort, Netherlands). System water was created using reverse
409 osmosis water kept at a pH of 7.2-7.6 with NaHCO₃ and coral sand and salt (Instant Ocean,
410 Blacksburg, VA) to maintain the conductivity at 600µS. Breeding of fish was carried out in 1-
411 2 L breeding tanks and embryos were collected in embryo medium (EM) (1.0mM MgSO₄,
412 0.15mM KH₂PO₄, 0.042mM Na₂HPO₄, 1mM CaCl₂, 0.5mM KCl, 15mM NaCl, 0.7mM
413 NaHCO₃) and raised in a dark incubator at 28.5 °C ⁸².

414 The following fish lines were used in the present project; AB fish from the Zebrafish
415 international resource centre (ZIRC) or was used for outbreeding and as wild-type background,
416 *appb*^{26,2-/-} ⁷ and *appa*^{-/-} as described below.

417 Human brain tissue samples were obtained from Queen Square Brain Bank for Neurological
418 Disorders, Department of Clinical and Movement Neurosciences, Institute of Neurology,
419 University College London (UCL). Ethical approval for the use of human post-mortem samples
420 was approved by a London Research Ethics Committee and tissue stored for research under a
421 license from the Human Tissue Authority with consent obtained from each donor. Human brain

422 tissues were used in accordance with the Helsinki declaration and the regional ethics
423 committees at UCL and the University of Gothenburg.

424

425 ***Mutagenesis using the CRISPR/Cas9 system***

426 Genetic mutations in the *appa* gene were introduced using the CRISPR/Cas9 system as
427 previously described⁸³. Briefly, gRNAs were generated with a target-specific DNA
428 oligonucleotide (Integrated DNA Technologies, Leuven, Belgium) containing a T7 promoter
429 sequence in the 5'-end and a ‘generic’ DNA oligonucleotide for the guide RNA. The two
430 oligonucleotides were annealed and extended with Platinum Taq DNA polymerase
431 (ThermoFisher, Waltham, MA), in a final concentration of 1x buffer, 0.25mM dNTP, 0.5μM
432 of each oligonucleotide and 0.04U/ul Taq with one cycle at the following temperatures (98°C
433 2 min; 50°C 10 min, 72°C 10 min). The resulting product was analyzed on a 2.5% agarose
434 (Roche, Basel, Switzerland) gel to confirm a single fragment of 120 basepairs (bp) and used to
435 transcribe RNA. *In vitro* transcription was performed with the T7 Quick High Yield RNA
436 Synthesis kit (New England Biolabs, Ipswich, MA) and incubated at 37°C for 16 h. DNA
437 template was removed with RNase Free DNase at 37°C for 15 min. After purification with the
438 RNA clean & concentrator-5 (Zymo Research, Irvine, CA), gRNA was analyzed on a 2.5%
439 agarose gel for integrity and diluted to 250μg/μl with RNase free water and stored at -80°C.
440 Cas9 protein was diluted to 500nM in Hepes (20mM HEPES, pH7.5; 150mM KCl) and stored
441 at -80°C. Embryos were co-injected with 50 pg gRNA and 300 pg Cas9 protein at the one to
442 two cell stage using a microinjector apparatus FemtoJet® express (Eppendorf AG, Hamburg,
443 Germany). Injected embryos were screened for gRNA activity using the T7 endonuclease assay
444 (New England Biolabs, Ipswich, MA). Ten embryos from each gRNA injection were pooled at
445 48 hpf and genomic DNA extracted with 50mM NaOH at 95°C for 30 min. M13- and PIG-
446 tailed primers (IDT, Leuven, Belgium) were used to amplify a region surrounding the mutated

447 site of each locus using 1x buffer, 2.5mM MgCl₂, 0.2mM dNTP, 0.2μM primers, 1U Taq
448 polymerase (Promega, Fitchburg, WI). The polymerase chain reaction (PCR) was purified on
449 an 1% agarose gel with the QIAquick Gel Extraction Kit (Quiagen, Hilden, Germany) and then
450 200 ng of the purified PCR product was dissociated and reannealed (95°C for 5min, 95-85°C
451 at -2°C /s, 85-25°C at 0.1°C /s) in a reaction containing 1x NEB buffer 2 (New England Biolabs,
452 Ipswich, MA) and then digested with 5U T7 endonuclease I (New England Biolabs, Ipswich,
453 MA) for one hour at 37°C. Fragments were analyzed on a 2% agarose gel. The remaining
454 embryos were raised to adulthood and outcrossed with AB wild-type fish. Sixteen embryos
455 from each outcrossed pair were screened for mutations in the F1 generation using a three-primer
456 fluorescence PCR method. A 300-450 bp region surrounding the target site was amplified using
457 forward primers linked with a M13 sequence and a PIG-tailed reverse primer in combination
458 with a generic M13-FAM primer. The *appa*^{C21-16} mutants, refer to as *appa*^{-/-}, carry a deletion
459 of -10 bp in exon 2. Sanger sequencing with BigDye™ Terminator v1.1 Cycle Sequencing Kit
460 (Applied Biosystems™, Waltham, MA) on an ABI3130xl sequencer (SeqGen Inc, Los
461 Angeles, CA) revealed a deletion of ten nucleotides in exon 2 that likely introduce a frameshift
462 mutations. Heterozygous mutant carriers were raised and subsequently outcrossed into the wild-
463 type AB fish line until generation F4. Outcrossed adults were genotyped using M13-FAM
464 primers and PCR reactions diluted in HiDi™ formamide (Applied Biosystems™, Waltham,
465 MA) with ROX™500 dye size ladder (ThermoFisher, Waltham, MA) and analyzed for
466 amplified fragment length polymorphism (AFLP) on an ABI3130xl sequencer. Offspring from
467 heterozygous F4 inbreds were inbred to generate homozygous wild-type and mutant lines.
468 Generation of *appa*^{-/-}*appb*^{-/-} double mutants were obtain from mating single mutant *appa*^{-/-} with
469 single mutant *appb*^{-/-}.

470

471 ***Protein sequence alignment***

472 Sequences of APP were obtained from the UniProt database⁸⁴ and aligned with ClustalW using
473 MegAlign Pro v17.2.1 (DNAstar, Inc., Madison, WI) The following sequences were used;
474 *Homo sapiens* APP751 (P05067-8), *Mus musculus* APP751 (P12023-3), *Danio rerio* Appa738
475 (Q90W28), Appb751 (B0V0E5). Amino acids conserved across all species were marked with
476 bright blue background.

477

478 ***Whole-mount fluorescent in situ hybridization***

479 To detect *appa* and *appb* mRNA expression pattern in zebrafish larvae, fluorescent *in situ*
480 hybridization was performed. Antisense digoxigenin-labeled *appa* and *appb* RNA probes used
481 are described previously⁸⁵. Zebrafish embryos were staged according to Kimmel *et al.* to the
482 hours post-fertilization (hpf)⁸⁶ and manually dechorionated with forceps (Dumont, Montignez,
483 Switzerland). A treatment with 0.003% PTU (1- phenyl-2-thiourea) (Sigma, St. Louis, MO)
484 was performed around 23hpf stage to prevent pigmentation. Fluorescent *in situ* hybridization
485 was performed as described by Lauter *et al.*⁸⁷. Briefly, zebrafish larvae were euthanized in
486 0.2mg/ml ethyl 3-aminobenzoate methanesulfonate (tricaine) (MS-222, Sigma, St. Louis, MO)
487⁸² and fixed at 30 hpf in 4% paraformaldehyde (PFA) (Sigma, St. Louis, MO) for 24h at 4°C.
488 Embryos were washed in phosphate-buffered saline (PBS) with 0.1%Tween-20 (PBST) and
489 dehydrate into increasing methanol (MeOH) gradients from 25 to 100%. Embryos were
490 incubated in 2% hydrogen peroxide (H₂O₂) for 20 min, then gradually rehydrated with
491 decreasing MeOH gradients. Embryos were incubated in 10µg/ml proteinase K (in 10mM Tris-
492 HCl pH 8.0, 1.0 mM EDTA) for 10 min at room temperature (RT). The reaction was stopped
493 with 2 mg/ml glycine in PBST and then the embryos were postfix in 4.0% PFA for 20 min.
494 PBST washes were performed before incubation in prehybridization buffer (HB; 50% deionized
495 formamide, 5x saline-sodium citrate (SSC) (3M NaCl, 300 mM tri-sodium citrate, pH 7.0), 5
496 mg/ml torula RNA (Sigma, St. Louis, MO), 50 µg/ml heparin sodium salt and 0.1% Tween-

497 20). Embryos were pre-hybridized at 70°C for 1h. Then, hybridization was done with
498 selectively 50 ng of DIG-labelled *appa* or *appb* RNA in HB with 5% dextran sulfate (Sigma,
499 St. Louis, MO) at 70 °C overnight. The next day, embryos were washed in warm SSC with
500 0.1% Tween-20 followed by PBST only. After that, a 1h-blocking incubation at RT in PBST
501 with 8% goat serum (Sigma, St. Louis, MO) was performed. For the antibody treatment, a
502 sheep-anti-digoxigenin-peroxidase (POD)-Fab fragments antibody (1:500 in blocking solution)
503 (Roche, Basel, Switzerland) was used and embryos were incubated in the dark overnight at 4°C,
504 without agitation. To remove excess antibody, embryos were then washed in PBST at RT in
505 gentle agitation. To amplify the signal, tyramide signal amplification (TSA) was used by
506 combining 5-carboxyfluorescein succinimidyl ester (Molecular Probes, Eugene, OR) with
507 tyramine hydrochlorine (Sigma, St. Louis, MO) at a 1.1:1 respective equimolar ratio. Vanillin
508 (0.45mg/mL) (Sigma, St. Louis, MO) was used as a POD accelerator and diluted in borate
509 buffer pH 8.5. Embryos were incubated with the TSA and POD accelerator reaction in the dark
510 without agitation for 15 min at RT. To stop the TSA reaction, embryos were washed in PBST
511 and then incubate in 100 mM glycine-HCl pH 2.0 to inactivate the POD reaction followed by
512 additional PBST washing. To avoid shrinkage, embryos were then incubated in an increasing
513 glycerol gradient (in PBST, 40mM NaHCO₃). Whole embryos were mounted on glass bottom
514 35 mm Petri dish (Cellvis, Mountain View, CA) in 1% low-melting agarose (Sigma, St. Louis,
515 MO). Samples were imaged as stacks using inverted Nikon A1 confocal system (Nikon
516 Instruments, Melville, NY) using a 20x objective (Plan-Apochromat 20x/0,75) and 40x water-
517 immersion objective (Apochromat LWD 40x/1,15). Image processing was done using ImageJ
518 FIJI software (NIH, Bethesda, MD).

519

520 ***Immunofluorescence***

521 *Zebrafish larvae*

522 To detect protein expression, immunofluorescence experiments were performed in whole-
523 mount AB zebrafish larvae. A treatment with 0.003% PTU was performed around 23hpf stage
524 to prevent pigmentation. Then freshly euthanized embryos were fixed at 30 hpf for 2h in 4%
525 PFA at RT on slow agitation. After fixation, embryos were washed with PBS with 0.5% Triton-
526 X (PBTx) at RT. Followed up by incubation in blocking solution (5% goat serum donor herd
527 (GS) (Sigma, St. Louis, MO), 2% bovine serum albumin (BSA) (Sigma, St. Louis, MO) , 1%
528 DMSO (Sigma, St. Louis, MO) and 0.5% PBTx) for 3h at RT. The larvae were then incubated
529 overnight at 4°C on slow agitation with the desired primary antibodies in blocking solution:
530 mouse IgG2b anti-acetylated tubulin monoclonal antibody (1:1000) (Sigma, St. Louis, MO),
531 recombinant rabbit anti-amyloid precursor protein monoclonal antibody Y188 (1:500) (Abcam,
532 Cambridge, United Kingdom), and/or mouse anti-glutamylated tubulin monoclonal antibody
533 (1:1000) (Adipogen, San Diego, CA). The zebrafish larvae used for negative control were
534 incubated in blocking solution only. The next day, embryos were washed (5x 45min) with
535 PBSTx at RT and incubated in dark with the specific secondary antibodies overnight at 4°C, in
536 blocking solution: goat anti-mouse IgG2b Alexa Fluor-647 (1:1000) (Invitrogen Thermo
537 Fisher, Waltham, MA) and goat anti-rabbit IgG Alexa Fluor-488 (1:1000) (Invitrogen Thermo
538 Fisher, Waltham, MA), or goat anti-mouse IgG1 Alexa Fluor-568 (1:1000) (Invitrogen Thermo
539 Fisher, Waltham, MA). The zebrafish larvae used for negative control were also incubated with
540 the former secondary antibodies. The larvae were then washed with PBTx at RT and incubated
541 for 15 min with DAPI (1:1000) (ThermoFisher, Waltham, MA) to stain the nuclei in PBS at RT
542 before the final washes. Stained larvae were mounted in 1% low-melting point agarose, on glass
543 bottom 35 mm Petri dish.

544 *Adult zebrafish and mouse brains*

545 Brains from adult zebrafish (AB, 2 year-old) and mouse (C57Bl6/n, 8-9 week-old). Brains were
546 fixed in 4% PFA in PBS overnight at 4°C and then washed and immersed in 30% sucrose
547 solution in PBS, after which they were frozen in OCT cryomount (Histolab, Askim, Sweden).
548 Coronal or sagittal cryosections from adult zebrafish (25 µm) and mouse brains (16 µm) slices
549 were stored at -80°C prior to use. Sections were air dried for 15 min at RT then rehydrated in
550 PBS. Slices were permeabilized in 0.1% PBTx for 10 min at RT and washed 3x in PBS for
551 15min each. A 0.1% Sudan Black B (SBB) (Sigma, St. Louis, MO) in 70% EtOH treatment
552 was performed for 20 min at RT. Slides were then washed in PBS for 3x5 min. The slides were
553 then incubated in blocking solution of 2% GS in PBS at RT for 1h, followed by the incubation
554 with the primary antibodies in 2% BSA at 4°C overnight: mouse IgG2b anti-acetylated tubulin
555 monoclonal antibody (1:1000), recombinant rabbit anti-amyloid precursor protein monoclonal
556 antibody (Y188) (1:500) or mouse anti-amyloid precursor protein A4 antibody (clone 22C11)
557 (1:500) (Merck Millipore, Burlington, MA), or rabbit IgG (1:500) (Abcam, Cambridge, United
558 Kingdom) and/or with blocking solution only for negative controls. The next day, slides were
559 wash 3x in PBS for 15min each and incubated with the secondary antibody in 2% BSA at RT
560 for 3.5h combined with DAPI (1:1000): goat anti-mouse IgG2b Alexa Fluor-647 (1:1000)
561 and/or goat-anti rabbit Alexa Fluor-488 (1:1000) and/or goat anti-mouse IgG1 Alexa Fluor-488
562 (1:1000) (ThermoFisher, Waltham, MA) and/or goat anti-mouse IgG1 Alexa Fluor-568
563 (1:1000). The slides were then washed 3x15 min in PBS and shortly rinsed in ddH₂O to remove
564 any residual salts. The slides were covered with coverslips using ProLong gold antifade
565 mounting medium (Invitrogen Thermo Fisher, Waltham, MA).

566 Samples were imaged using Zeiss LSM710 inverted confocal microscope (Carl-Zeiss, Jena,
567 Germany) using 40x water immersion objective (Plan-Apochromat 40x/1.0) and a 63x oil-
568 immersion objective (Plan-Apochromat 40x/1.0) or with Zeiss LSM880 Airyscan inverted
569 confocal microscope (Carl-Zeiss, Jena, Germany) using 40x water immersion objective (LCD-

570 Apochromat 40x/1.0) and 63x oil-immersion objective (Plan-Apochromat 63x/1.4). Image
571 processing and intensity profiles were performed with ImageJ FIJI program.

572

573 ***Human brain sections immunofluorescent staining***

574 Neurologically normal human post-mortem control tissue was obtained from Queen Square
575 Brain Bank for Neurological Studies. Paraffin-embedded sections were cut from caudate
576 nucleus brain region, which contains ependymal lining containing cilia. Sections were dewaxed
577 in three changes of xylene and rehydrated using graded alcohols. Endogenous peroxidase
578 activity was blocked using 0.3% H₂O₂ in MeOH for 10 min followed by pressure cooker pre-
579 treatment for 10 min in citrate buffer, pH 6.0. Non-specific binding was blocked using 10%
580 non-fat dried milk (Sigma-Aldrich, St. Louis, MO) in Tris buffered saline-Tween (TBS-Tween)
581 before incubating with either anti-acetylated tubulin (1:1000) or anti-APP (1:500) antibodies at
582 RT for 1 h. A biotinylated mouse anti-rabbit IgG antibody (1:200) (Agilent DAKO, Glostrup,
583 Denmark) was added for a 30 min incubation with the sections at RT followed by avidin-biotin
584 complex (Vector Laboratories, Burlingame, CA). Coloration was developed with di-
585 aminobenzidine (Sigma-Aldrich, St. Louis, MO) activated with H₂O₂⁸⁸.

586

587 ***Protein extraction from whole zebrafish larvae and western blotting***

588 Protein was extracted from 3dpf double *appa*^{-/-}*appb*^{-/-} mutant whole larvae (60 larvae per n,
589 n=3) to confirm loss of protein. Larvae were euthanized, deyolked with ice-cold PBS and snap
590 frozen in liquid nitrogen prior to use and stored at -80°C. Samples were homogenized in an ice-
591 cold lysis buffer (10 mM Tris-HCl pH 8.0, 2% sodium deoxycholate, 2% SDS, 1 mM EDTA,
592 0.5 M NaCl, 15% glycerol) supplemented with protease inhibitors cocktail (Roche, Basel,
593 Switzerland) and using glass tissue grinder, on ice. Samples were then incubated 20 min on ice,

594 sonicated for 10 min on max level and centrifuged at 10,000 x g at 4°C. Supernatants were
595 collected and kept on ice and protein concentration measured with a BCA Protein Assay Kit
596 (ThermoFisher, Waltham, MA) and samples stored at -80°C. Proteins samples (40-60ug) were
597 then diluted in a denaturing lysis buffer (1X NuPAGE® LDS Sample Buffer (ThermoFisher,
598 Waltham, MA), 0.05M DTT (Sigma-Aldrich, St. Louis, MO), lysis buffer completed with
599 protease inhibitors) and then boiled for 5 min at 95°C. Proteins were then separated on a
600 NuPAGE® NOVEX® Bis-TRIS pre-cast gel (Invitrogen Thermo Fisher, Waltham, MA) and
601 transferred onto a 0.2 µm nitrocellulose membrane (GE Healthcare, Chicago, IL). The
602 membrane was incubated in a blocking solution (5% milk) for 2h at RT and then immunoblotted
603 with the desired primary antibodies overnight at 4°C: rabbit anti-amyloid precursor protein
604 monoclonal antibody (Y188) (1:2000) or mouse anti-amyloid precursor protein A4 antibody
605 (clone 22C11) (1:5000) and with a loading concentration control mouse anti-GAPDH-HRP
606 conjugated (1:20000) (Novus Biologicals, Centennial, CO) or mouse anti- α -tubulin monoclonal
607 (1:10000) (Sigma, St. Louis, MO). The membrane was then washed in TBS-Tween 3x 10min
608 at RT and incubated with the secondary antibodies anti-rabbit-HRP (1:5000) (Cell Signaling,
609 Danvers, MA) for 1h at RT. The membrane was washed 3x10min in TBS-Tween before being
610 developed. The signal was developed using SuperSignal West Dura Extended Duration
611 Substrate kit (ThermoFisher, Waltham, MA) and imaged using ChemiDoc Imaging (Bio-Rad,
612 Hercules, CA). Western blot images were processed and analysed using Image Lab program
613 (Bio-Rad, Hercules, CA). Quantification of band intensities were performed by Image Lab
614 (Bio-Rad, Hercules, CA) with GAPDH or alpha-tubulin used to control protein loading.
615 Samples were normalized to controls.

616

617 ***RNA extraction from whole zebrafish larvae and qPCR***

618 To confirm *appa* and *appb* mRNA levels decrease in our double mutant (*appa*^{-/-}*appb*^{-/-}), RNA
619 was extracted from 24 hpf whole larvae (10 larvae per n, n=5). Total RNA was extracted using
620 TRI Reagent[®] (Sigma, St. Louis, MO). Then, RNA samples were treated with RQ1 RNase-free
621 DNase 1x reaction buffer and RQ1 RNase-free DNase (Promega, Fitchburg, WI). cDNA was
622 synthesized using High-Capacity RNA-to-cDNATM Kit (Applied BiosystemsTM, Waltham,
623 MA) with RNase inhibitor and converted in a single-cycle reaction on a 2720 Thermal Cycler
624 (Applied BiosystemsTM, Waltham, MA). Quantitative PCR was performed with inventoried
625 TaqMan Gene Expression Assays with FAM reporter dye in TaqMan Universal PCR Master
626 Mix with UNG (ThermoFisher, Waltham, MA). The assay was carried out on Micro-Amp 96-
627 well optical microtiter plates (ThermoFisher, Waltham, MA) on a 7900HT Fast QPCR System
628 (Applied BiosystemsTM, Waltham, MA). qPCR results were analysed with the SDS 2.3 software
629 (Applied BiosystemsTM, Waltham, MA). cDNA values from each sample was normalized with
630 average C_T's of house-keeping genes (*eef1a1l1* and *actb1*), then the relative quantity was
631 determined using the ΔΔC_T method⁸⁹ with the sample of wild-type sibling embryos (24 hpf) as
632 the calibrator. TaqMan[®] Gene Expression Assays (Applied BiosystemsTM, Waltham, MA) were
633 used for the following genes: amyloid beta (A4) precursor protein A (*appa*) (Dr03144365_m1),
634 eukaryotic translation elongation factor 1 alpha 1, like 1 (*eef1a1l1*) (Dr03432748_m1) and
635 actin, beta 1 (*actb1*) (Dr03432610_m1).

636

637 ***Cilia length measurement in zebrafish larvae***

638 To compare the number of brain ependymal cilia and their length, 30 hpf AB wild-type and
639 *appa*^{-/-}*appb*^{-/-} zebrafish larvae were used. The larvae were treated with PTU, fixed in 4% PFA
640 and the immunostaining with antibody against acetylated tubulin was performed as describe in
641 the section above. Stacks (of around 25μm depending on the angle of the mounted sample) were
642 taken in the region of interest (ROI) of the dorsal portion of the diencephalic ventricle using

643 Zeiss LSM710 confocal microscope using inverted 40x water immersion objective (Plan-
644 Apochromat 40x/1.0). Images were then processed using Imaris (BITPLANE™, Belfast,
645 United Kingdom) and the cilia length was measured with the acetylated tubulin signal using the
646 “measuring points” tool of the program. Raw data of the measurement were exported to
647 Microsoft Excel and compiled into GraphPad Prism® 7 for statistical analysis.

648 ***Brain ventricles injection and size measurement***

649 To measure the size of the brain ventricles in live zebrafish, 2dpf PTU-treated zebrafish larvae
650 were used. Rhodamine-Dextran injection protocol was performed as describe by Gutzman and
651 Sive⁹⁰. Briefly, the larvae were anesthetized with tricaine in the EM and transferred onto a Petri
652 dish covered with 1% agarose, lined with rows moulded. The larvae were kept in EM
653 complemented with tricaine during the whole procedure and place on a ventral position, with
654 top of their head facing upwards. Injections were performed using borosilicate injection needles
655 previously pulled (P-97 Flaming/Brown micropipette puller) (Sutter Instrument, Novato, CA).
656 Using a microinjector apparatus, 2nl of Rhodamine B isothiocyanate-Dextran (Sigma, St.
657 Louis, MO) were injected in the hindbrain ventricle without perforating or hitting the brain
658 tissue below.

659 Larvae with non-effective injections were sorted out using a fluorescent stereomicroscope
660 (Nikon Instruments, Melville, NY). Quickly after the sorting, the larvae were mounted in 1%
661 low-melting point agarose on glass bottom 35 mm Petri dish. Confocal imaging stacks were
662 acquired using an inverted Nikon A1 confocal system using a 20x objective (Plan-Apochromat
663 20x/0,75). Image processing of the confocal stacks were done with Imaris program. The
664 “surface” tool option was used for each sample. Data of the surface volume and area were
665 automatically generated by the program. Length measurements of the areas of the ventricles
666 were obtain manually with the “measuring tool”. All data were exported into Microsoft Excel
667 and GraphPad® 7 Prism for statistical analysis.

668 ***Transmission electron microscopy***

669 To evaluate the integrity of the internal structure of the axonemes and microtubules doublets of
670 the brain motile cilia in older zebrafish, transmission electron microscopy was performed on
671 fixed brains. Adult zebrafish were euthanized in tricaine and brains dissected, rinsed in ice-cold
672 PBS and fixed in 2% PFA and 2% glutaraldehyde (Sigma, St. Louis, MO), in 0.042M Millonig
673 buffer (0.081M Na₂HPO₄, 0.0183M NaH₂PO₄, 0.086M NaCl) pH 7.4 at least 24h at 4°C. After
674 fixation, brains were cut in two halves and then treated in 2% osmium tetroxide (Sigma, St.
675 Louis, MO) in 0.1M Millonig buffer pH 7.4. Specimens were then rinsed and incubated
676 overnight in 4% sucrose solution in 0.1M Millonig buffer pH 7.4 after which they were
677 dehydrated in series of ethanol and embedded in a mix of acetone and agar 100 resin plastic
678 (TAAB Laboratories Equipment Ltd, Berks, United Kingdom) and allowed to polymerize for
679 48h. Blocks were trimmed as semi-thin (1 µm) and ultra-thin (70 nm) sections collected with a
680 commercial ultramicrotome (Leica EM UC7, Leica Microsystems, Wetzlar, Germany).
681 Sections were post-stained with 5% uranyl acetate in distilled H₂O during 40-60 min, rinsed in
682 distilled H₂O and then treated with 0.3% Lead Citrate (ThermoFisher, Waltham, MA) for 30-
683 60 s. Images were acquired using secondary electron detection. Images were acquired with a
684 Tecnai Spirit BT transmission electron microscope (Field Electron and Ion Company,
685 Hillsboro, OR).

686

687 ***Statistical analysis***

688 Statistical analysis was performed using GraphPad 7 software (Prism®, San Diego, CA). Data
689 were presented as means with standard deviation (\pm SD) or standard errors of the mean (\pm
690 SEM). For analysis of cilia length, D'Agostino & Pearson normality test ($P < 0.0001$) and non-
691 parametric two-tailed Mann-Whitney U tests were performed. Results related to qPCR and
692 western blot quantification, and ventricle size measurements were compared statistically using

693 unpaired Student's t-tests. Statistical significance was set at $p < 0.05$ (*), 0.01 (**), 0.005 (***)
694 and 0.0001 (****).

695

696 **Data availability**

697 The datasets generated during and/or analysed during the current study are available from the
698 corresponding author on reasonable request.

699

700 **References**

- 701 1 Selkoe, D. J. & Hardy, J. The amyloid hypothesis of Alzheimer's disease at 25 years.
702 *EMBO Mol Med* **8**, 595-608, doi:10.15252/emmm.201606210 (2016).
- 703 2 Blennow, K., de Leon, M. J. & Zetterberg, H. Alzheimer's disease. *The Lancet* **368**, 387-
704 403, doi:10.1016/s0140-6736(06)69113-7 (2006).
- 705 3 Wang, B. *et al.* The Amyloid Precursor Protein Controls Adult Hippocampal
706 Neurogenesis through GABAergic Interneurons. *Journal of Neuroscience* **34**, 13314-
707 13325, doi:10.1523/jneurosci.2848-14.2014 (2014).
- 708 4 Caille, I. *et al.* Soluble form of amyloid precursor protein regulates proliferation of
709 progenitors in the adult subventricular zone. *Development* **131**, 2173-2181,
710 doi:10.1242/dev.01103 (2004).
- 711 5 Young-Pearse, T. L., Chen, A. C., Chang, R., Marquez, C. & Selkoe, D. J. Secreted APP
712 regulates the function of full-length APP in neurite outgrowth through interaction with
713 integrin beta1. *Neural Dev* **3**, 15, doi:10.1186/1749-8104-3-15 (2008).
- 714 6 Deyts, C., Thinakaran, G. & Parent, A. T. APP Receptor? To Be or Not To Be. *Trends
715 Pharmacol Sci* **37**, 390-411, doi:10.1016/j.tips.2016.01.005 (2016).
- 716 7 Banote, R. K. *et al.* Amyloid precursor protein-b facilitates cell adhesion during early
717 development in zebrafish. *Sci Rep* **10**, 10127, doi:10.1038/s41598-020-66584-8 (2020).
- 718 8 Wang, Z. *et al.* Presynaptic and postsynaptic interaction of the amyloid precursor
719 protein promotes peripheral and central synaptogenesis. *J Neurosci* **29**, 10788-10801,
720 doi:10.1523/JNEUROSCI.2132-09.2009 (2009).
- 721 9 Young-Pearse, T. L. *et al.* A Critical Function for -Amyloid Precursor Protein in
722 Neuronal Migration Revealed by In Utero RNA Interference. *Journal of Neuroscience*
723 **27**, 14459-14469, doi:10.1523/jneurosci.4701-07.2007 (2007).
- 724 10 Muller, U. C., Deller, T. & Korte, M. Not just amyloid: physiological functions of the
725 amyloid precursor protein family. *Nat Rev Neurosci* **18**, 281-298,
726 doi:10.1038/nrn.2017.29 (2017).
- 727 11 Haass, C., Kaether, C., Thinakaran, G. & Sisodia, S. Trafficking and proteolytic
728 processing of APP. *Cold Spring Harb Perspect Med* **2**, a006270,
729 doi:10.1101/cshperspect.a006270 (2012).
- 730 12 Brown, J. M. & Witman, G. B. Cilia and Diseases. *Bioscience* **64**, 1126-1137,
731 doi:10.1093/biosci/biu174 (2014).

- 732 13 Park, S. M., Jang, H. J. & Lee, J. H. Roles of Primary Cilia in the Developing Brain.
733 *Front Cell Neurosci* **13**, 218, doi:10.3389/fncel.2019.00218 (2019).
- 734 14 Spassky, N. *et al.* Adult ependymal cells are postmitotic and are derived from radial
735 glial cells during embryogenesis. *J Neurosci* **25**, 10-18,
736 doi:10.1523/JNEUROSCI.1108-04.2005 (2005).
- 737 15 Lechtreck, K. F., Delmotte, P., Robinson, M. L., Sanderson, M. J. & Witman, G. B.
738 Mutations in Hydin impair ciliary motility in mice. *J Cell Biol* **180**, 633-643,
739 doi:10.1083/jcb.200710162 (2008).
- 740 16 Abbott, N. J., Pizzo, M. E., Preston, J. E., Janigro, D. & Thorne, R. G. The role of brain
741 barriers in fluid movement in the CNS: is there a 'glymphatic' system? *Acta Neuropathol*
742 **135**, 387-407, doi:10.1007/s00401-018-1812-4 (2018).
- 743 17 Ethell, D. W. Disruption of cerebrospinal fluid flow through the olfactory system may
744 contribute to Alzheimer's disease pathogenesis. *J Alzheimers Dis* **41**, 1021-1030,
745 doi:10.3233/JAD-130659 (2014).
- 746 18 Kapoor, K. G., Katz, S. E., Grzybowski, D. M. & Lubow, M. Cerebrospinal fluid
747 outflow: an evolving perspective. *Brain Res Bull* **77**, 327-334,
748 doi:10.1016/j.brainresbull.2008.08.009 (2008).
- 749 19 Klein, S. *et al.* Truncating mutations in APP cause a distinct neurological phenotype.
750 *Ann Neurol* **80**, 456-460, doi:10.1002/ana.24727 (2016).
- 751 20 Kiprilov, E. N. *et al.* Human embryonic stem cells in culture possess primary cilia with
752 hedgehog signaling machinery. *J Cell Biol* **180**, 897-904, doi:10.1083/jcb.200706028
753 (2008).
- 754 21 Magara, F. *et al.* Genetic background changes the pattern of forebrain commissure
755 defects in transgenic mice underexpressing the -amyloid-precursor protein.
756 *Proceedings of the National Academy of Sciences* **96**, 4656-4661,
757 doi:10.1073/pnas.96.8.4656 (1999).
- 758 22 Baudoin, J. P. *et al.* Tangentially migrating neurons assemble a primary cilium that
759 promotes their reorientation to the cortical plate. *Neuron* **76**, 1108-1122,
760 doi:10.1016/j.neuron.2012.10.027 (2012).
- 761 23 Guo, J. *et al.* Primary Cilia Signaling Shapes the Development of Interneuronal
762 Connectivity. *Dev Cell* **42**, 286-300 e284, doi:10.1016/j.devcel.2017.07.010 (2017).
- 763 24 Higinbotham, H. *et al.* Arl13b-regulated cilia activities are essential for polarized
764 radial glial scaffold formation. *Nat Neurosci* **16**, 1000-1007, doi:10.1038/nn.3451
765 (2013).
- 766 25 Guo, J. *et al.* Primary Cilia Signaling Promotes Axonal Tract Development and Is
767 Disrupted in Joubert Syndrome-Related Disorders Models. *Developmental Cell* **51**, 759-
768 774.e755, doi:10.1016/j.devcel.2019.11.005 (2019).
- 769 26 Galati, D. F., Sullivan, K. D., Pham, A. T., Espinosa, J. M. & Pearson, C. G. Trisomy
770 21 Represses Cilia Formation and Function. *Dev Cell* **46**, 641-650 e646,
771 doi:10.1016/j.devcel.2018.07.008 (2018).
- 772 27 Chakravarthy, B. *et al.* Reduction of the immunostainable length of the hippocampal
773 dentate granule cells' primary cilia in 3xAD-transgenic mice producing human A β 1-42
774 and tau. *Biochemical and Biophysical Research Communications* **427**, 218-222,
775 doi:10.1016/j.bbrc.2012.09.056 (2012).
- 776 28 Ibanez-Tallón, I. *et al.* Dysfunction of axonemal dynein heavy chain Mdnah5 inhibits
777 ependymal flow and reveals a novel mechanism for hydrocephalus formation. *Hum Mol
778 Genet* **13**, 2133-2141, doi:10.1093/hmg/ddh219 (2004).
- 779 29 Vorobyeva, A. G. & Saunders, A. J. Amyloid-beta interrupts canonical Sonic hedgehog
780 signaling by distorting primary cilia structure. *Cilia* **7**, 5, doi:10.1186/s13630-018-0059-
781 y (2018).

- 782 30 Musa, A., Lehrach, H. & Russo, V. A. Distinct expression patterns of two zebrafish
783 homologues of the human APP gene during embryonic development. *Dev Genes Evol*
784 **211**, 563-567, doi:10.1007/s00427-001-0189-9 (2001).
- 785 31 Tanimoto, M., Ota, Y., Inoue, M. & Oda, Y. Origin of inner ear hair cells:
786 morphological and functional differentiation from ciliary cells into hair cells in
787 zebrafish inner ear. *J Neurosci* **31**, 3784-3794, doi:10.1523/JNEUROSCI.5554-10.2011
788 (2011).
- 789 32 Kawarabayashi, T., Shoji, M., Harigaya, Y., Yamaguchi, H. & Hirai, S. Amyloid
790 beta/A4 protein precursor is widely distributed in both the central and peripheral
791 nervous systems of the mouse. *Brain Res* **552**, 1-7, doi:10.1016/0006-8993(91)90651-
792 b (1991).
- 793 33 Ohta, M. *et al.* Immunohistochemical distribution of amyloid precursor protein during
794 normal rat development. *Brain Res Dev Brain Res* **75**, 151-161, doi:10.1016/0165-
795 3806(93)90019-7 (1993).
- 796 34 Stern, R. A., Otvos, L., Jr., Trojanowski, J. Q. & Lee, V. M. Monoclonal antibodies to
797 a synthetic peptide homologous with the first 28 amino acids of Alzheimer's disease
798 beta-protein recognize amyloid and diverse glial and neuronal cell types in the central
799 nervous system. *Am J Pathol* **134**, 973-978 (1989).
- 800 35 Fame, R. M., Chang, J. T., Hong, A., Aponte-Santiago, N. A. & Sive, H. Directional
801 cerebrospinal fluid movement between brain ventricles in larval zebrafish. *Fluids*
802 *Barriers CNS* **13**, 11, doi:10.1186/s12987-016-0036-z (2016).
- 803 36 Manton I.; Clarke, B. An electron microscope study of the spermatozoid of sphagnum.
804 *Journal of Experimental Botany* **3**, 265-275 (1952).
- 805 37 Satir, P. Studies on cilia: II. Examination of the distal region of the ciliary shaft and the
806 role of the filaments in motility. *Journal of Cell Biology*, 805-834 (1965).
- 807 38 Satir, P., Heuser, T. & Sale, W. S. A Structural Basis for How Motile Cilia Beat.
808 *Bioscience* **64**, 1073-1083, doi:10.1093/biosci/biu180 (2014).
- 809 39 Tam, B. M., Moritz, O. L., Hurd, L. B. & Papermaster, D. S. Identification of an outer
810 segment targeting signal in the COOH terminus of rhodopsin using transgenic Xenopus
811 laevis. *J Cell Biol* **151**, 1369-1380, doi:10.1083/jcb.151.7.1369 (2000).
- 812 40 Deretic, D. A role for rhodopsin in a signal transduction cascade that regulates
813 membrane trafficking and photoreceptor polarity. *Vision Research* **46**, 4427-4433,
814 doi:10.1016/j.visres.2006.07.028 (2006).
- 815 41 Rakoczy, E. P., Kiel, C., McKeone, R., Stricher, F. & Serrano, L. Analysis of disease-
816 linked rhodopsin mutations based on structure, function, and protein stability
817 calculations. *J Mol Biol* **405**, 584-606, doi:10.1016/j.jmb.2010.11.003 (2011).
- 818 42 Berbari, N. F., Johnson, A. D., Lewis, J. S., Askwith, C. C. & Mykytyn, K. Identification
819 of ciliary localization sequences within the third intracellular loop of G protein-coupled
820 receptors. *Mol Biol Cell* **19**, 1540-1547, doi:10.1091/mbc.E07-09-0942 (2008).
- 821 43 Domire, J. S. *et al.* Dopamine receptor 1 localizes to neuronal cilia in a dynamic process
822 that requires the Bardet-Biedl syndrome proteins. *Cell Mol Life Sci* **68**, 2951-2960,
823 doi:10.1007/s00018-010-0603-4 (2011).
- 824 44 Chakravarthy, B. *et al.* The p75 neurotrophin receptor is localized to primary cilia in
825 adult murine hippocampal dentate gyrus granule cells. *Biochem Biophys Res Commun*
826 **401**, 458-462, doi:10.1016/j.bbrc.2010.09.081 (2010).
- 827 45 Ye, F. *et al.* Single molecule imaging reveals a major role for diffusion in the exploration
828 of ciliary space by signaling receptors. *eLife* **2**, doi:10.7554/elife.00654 (2013).

- 829 46 de Coninck, D., Schmidt, T. H., Schloetel, J. G. & Lang, T. Packing Density of the
830 Amyloid Precursor Protein in the Cell Membrane. *Biophys J* **114**, 1128-1141,
831 doi:10.1016/j.bpj.2018.01.009 (2018).
- 832 47 Yang, J. & Li, T. The ciliary rootlet interacts with kinesin light chains and may provide
833 a scaffold for kinesin-1 vesicular cargos. *Exp Cell Res* **309**, 379-389,
834 doi:10.1016/j.yexcr.2005.05.026 (2005).
- 835 48 Long, H. & Huang, K. Transport of Ciliary Membrane Proteins. *Frontiers in Cell and
836 Developmental Biology* **7**, doi:10.3389/fcell.2019.00381 (2020).
- 837 49 Malicki, J. & Avidor-Reiss, T. From the cytoplasm into the cilium: bon voyage. *Organogenesis* **10**, 138-157, doi:10.4161/org.29055 (2014).
- 838 50 Mita, S., Schon, E. A. & Herbert, J. Widespread expression of amyloid beta-protein
839 precursor gene in rat brain. *Am J Pathol* **134**, 1253-1261 (1989).
- 840 51 Alvarez-Buylla, A. & Lim, D. A. For the long run: maintaining germinal niches in the
841 adult brain. *Neuron* **41**, 683-686, doi:10.1016/s0896-6273(04)00111-4 (2004).
- 842 52 Zhang, X. et al. Cilia-driven cerebrospinal fluid flow directs expression of urotensin
843 neuropeptides to straighten the vertebrate body axis. *Nat Genet* **50**, 1666-1673,
844 doi:10.1038/s41588-018-0260-3 (2018).
- 845 53 Song, Z., Zhang, X., Jia, S., Yelick, P. C. & Zhao, C. Zebrafish as a Model for Human
846 Ciliopathies. *J Genet Genomics* **43**, 107-120, doi:10.1016/j.jgg.2016.02.001 (2016).
- 847 54 Lowery, L. A., De Rienzo, G., Gutzman, J. H. & Sive, H. Characterization and
848 classification of zebrafish brain morphology mutants. *Anat Rec (Hoboken)* **292**, 94-106,
849 doi:10.1002/ar.20768 (2009).
- 850 55 Lowery, L. A. & Sive, H. Initial formation of zebrafish brain ventricles occurs
851 independently of circulation and requires the nagie oko and snakehead/atp1a1a.1 gene
852 products. *Development* **132**, 2057-2067, doi:10.1242/dev.01791 (2005).
- 853 56 Olstad, E. W. et al. Ciliary Beating Compartmentalizes Cerebrospinal Fluid Flow in the
854 Brain and Regulates Ventricular Development. *Curr Biol* **29**, 229-241 e226,
855 doi:10.1016/j.cub.2018.11.059 (2019).
- 856 57 Sawamoto, K. New Neurons Follow the Flow of Cerebrospinal Fluid in the Adult Brain.
857 *Science* **311**, 629-632, doi:10.1126/science.1119133 (2006).
- 858 58 Demars, M., Hu, Y. S., Gadadhar, A. & Lazarov, O. Impaired neurogenesis is an early
859 event in the etiology of familial Alzheimer's disease in transgenic mice. *J Neurosci Res*
860 **88**, 2103-2117, doi:10.1002/jnr.22387 (2010).
- 861 59 Ma, Q. H., Bagnard, D., Xiao, Z. C. & Dawe, G. S. A TAG on to the neurogenic
862 functions of APP. *Cell Adh Migr* **2**, 2-8, doi:10.4161/cam.2.1.5790 (2008).
- 863 60 Giacomini, A. et al. Inhibition of APP gamma-secretase restores Sonic Hedgehog
864 signaling and neurogenesis in the Ts65Dn mouse model of Down syndrome. *Neurobiol
865 Dis* **82**, 385-396, doi:10.1016/j.nbd.2015.08.001 (2015).
- 866 61 Clement, A., Solnica-Krezel, L. & Gould, K. L. The Cdc14B phosphatase contributes
867 to ciliogenesis in zebrafish. *Development* **138**, 291-302, doi:10.1242/dev.055038
868 (2011).
- 869 62 Fame, R. M. & Lehtinen, M. K. Emergence and Developmental Roles of the
870 Cerebrospinal Fluid System. *Dev Cell* **52**, 261-275, doi:10.1016/j.devcel.2020.01.027
871 (2020).
- 872 63 Zappaterra, M. W. & Lehtinen, M. K. The cerebrospinal fluid: regulator of
873 neurogenesis, behavior, and beyond. *Cell Mol Life Sci* **69**, 2863-2878,
874 doi:10.1007/s00018-012-0957-x (2012).
- 875 64 LeMay, M. & Alvarez, N. The relationship between enlargement of the temporal horns
876 of the lateral ventricles and dementia in aging patients with Down syndrome.
877 *Neuroradiology* **32**, 104-107, doi:10.1007/bf00588558 (1990).

- 879 65 Ezratty, E. J., Pasolli, H. A. & Fuchs, E. A Presenilin-2-ARF4 trafficking axis modulates
880 Notch signaling during epidermal differentiation. *J Cell Biol* **214**, 89-101,
881 doi:10.1083/jcb.201508082 (2016).
- 882 66 Nager, A. R. *et al.* An Actin Network Dispatches Ciliary GPCRs into Extracellular
883 Vesicles to Modulate Signaling. *Cell* **168**, 252-263 e214,
884 doi:10.1016/j.cell.2016.11.036 (2017).
- 885 67 Perez-Gonzalez, R., Gauthier, S. A., Kumar, A. & Levy, E. The exosome secretory
886 pathway transports amyloid precursor protein carboxyl-terminal fragments from the cell
887 into the brain extracellular space. *J Biol Chem* **287**, 43108-43115,
888 doi:10.1074/jbc.M112.404467 (2012).
- 889 68 Spitzer, P. *et al.* Microvesicles from cerebrospinal fluid of patients with Alzheimer's
890 disease display reduced concentrations of tau and APP protein. *Sci Rep* **9**, 7089,
891 doi:10.1038/s41598-019-43607-7 (2019).
- 892 69 Leinonen, V., Kuulasmaa, T. & Hiltunen, M. iNPH-the mystery resolving. *EMBO Mol
Med* **13**, e13720, doi:10.15252/emmm.202013720 (2021).
- 894 70 Jeppsson, A., Zetterberg, H., Blennow, K. & Wikkelsø, C. Idiopathic normal-pressure
895 hydrocephalus: pathophysiology and diagnosis by CSF biomarkers. *Neurology* **80**,
896 1385-1392, doi:10.1212/WNL.0b013e31828c2fda (2013).
- 897 71 Jeppsson, A. *et al.* Amyloid mis-metabolism in idiopathic normal pressure
898 hydrocephalus. *Fluids Barriers CNS* **13**, 13, doi:10.1186/s12987-016-0037-y (2016).
- 899 72 Pyykko, O. T. *et al.* Cerebrospinal fluid biomarker and brain biopsy findings in
900 idiopathic normal pressure hydrocephalus. *PLoS One* **9**, e91974,
901 doi:10.1371/journal.pone.0091974 (2014).
- 902 73 Kim, J. Y. *et al.* Distinct amyloid precursor protein processing machineries of the
903 olfactory system. *Biochem Biophys Res Commun* **495**, 533-538,
904 doi:10.1016/j.bbrc.2017.10.153 (2018).
- 905 74 Reiten, I. *et al.* Motile-Cilia-Mediated Flow Improves Sensitivity and Temporal
906 Resolution of Olfactory Computations. *Curr Biol* **27**, 166-174,
907 doi:10.1016/j.cub.2016.11.036 (2017).
- 908 75 Miyasaka, N. *et al.* Functional development of the olfactory system in zebrafish. *Mech
Dev* **130**, 336-346, doi:10.1016/j.mod.2012.09.001 (2013).
- 910 76 Miyasaka, N. *et al.* Robo2 is required for establishment of a precise glomerular map in
911 the zebrafish olfactory system. *Development* **132**, 1283-1293, doi:10.1242/dev.01698
912 (2005).
- 913 77 Doty, R. L. The olfactory system and its disorders. *Semin Neurol* **29**, 74-81,
914 doi:10.1055/s-0028-1124025 (2009).
- 915 78 Trudeau, S. *et al.* Diagnosis and patterns of hearing loss in children with severe
916 developmental delay. *Am J Otolaryngol* **42**, 102923, doi:10.1016/j.amjoto.2021.102923
917 (2021).
- 918 79 Liu, Y. *et al.* Hearing loss is an early biomarker in APP/PS1 Alzheimer's disease mice.
919 *Neurosci Lett* **717**, 134705, doi:10.1016/j.neulet.2019.134705 (2020).
- 920 80 Omata, Y. *et al.* Expression of amyloid- β in mouse cochlear hair cells causes an early-
921 onset auditory defect in high-frequency sound perception. *Aging* **8**, 427-439,
922 doi:10.18632/aging.100899 (2016).
- 923 81 Kilkenny, C., Browne, W. J., Cuthill, I. C., Emerson, M. & Altman, D. G. Improving
924 bioscience research reporting: the ARRIVE guidelines for reporting animal research.
925 *PLoS Biol* **8**, e1000412, doi:10.1371/journal.pbio.1000412 (2010).
- 926 82 Westerfield, M. The Zebrafish Book : A Guide for the Laboratory Use of Zebrafish.
927 http://zfin.org/zf_info/zfbook/zfbk.html (2000).

- 928 83 Varshney, G. K. *et al.* A high-throughput functional genomics workflow based on
929 CRISPR/Cas9-mediated targeted mutagenesis in zebrafish. *Nature protocols* **11**, 2357-
930 2375, doi:10.1038/nprot.2016.141 (2016).
- 931 84 UniProt, C. UniProt: the universal protein knowledgebase in 2021. *Nucleic Acids Res*
932 **49**, D480-D489, doi:10.1093/nar/gkaa1100 (2021).
- 933 85 Banote, R. K. *et al.* Amyloid precursor protein-b facilitates cell adhesion during early
934 development in zebrafish. *Sci. Rep.* **10**, 10127, doi:10.1038/s41598-020-66584-8
935 (2020).
- 936 86 Kimmel, C. B., Ballard, W. W., Kimmel, S. R., Ullmann, B. & Schilling, T. F. Stages
937 of embryonic development of the zebrafish. *Dev Dyn* **203**, 253-310,
938 doi:10.1002/aja.1002030302 (1995).
- 939 87 Lauter, G., Söll, I. & Hauptmann, G. Sensitive whole-mount fluorescent in situ
940 hybridization in zebrafish using enhanced tyramide signal amplification. *Methods Mol.*
941 *Biol.* **1082**, 175-185, doi:10.1007/978-1-62703-655-9_12 (2014).
- 942 88 Lashley, T. *et al.* A comparative clinical, pathological, biochemical and genetic study
943 of fused in sarcoma proteinopathies. *Brain* **134**, 2548-2564, doi:10.1093/brain/awr160
944 (2011).
- 945 89 Livak, K. J. & Schmittgen, T. D. Analysis of relative gene expression data using real-
946 time quantitative PCR and the 2(-Delta Delta C(T)) Method. *Methods (San Diego,*
947 *Calif.)* **25**, 402-408, doi:10.1006/meth.2001.1262 (2001).
- 948 90 Gutzman, J. H. & Sive, H. Zebrafish brain ventricle injection. *J Vis Exp*,
949 doi:10.3791/1218 (2009).

950

951 Acknowledgements

952 We thank Elisa Alexandersson and Katarina Turner Stenström for fish maintenance and the
953 Centre for Cellular Imaging at the University of Gothenburg and the National Microscopy
954 Infrastructure (VR-RFI 2016-00968) for microscopy support. We also thank Debora Kaminski
955 for the mouse brains samples, Nathalie Jurish-Yaksi (Norwegian University of Science and
956 Technology – NTNU) and Jean-François Papon (Public Hospital Network of Paris (AP-HP))
957 for insight and thoughtful discussions about cilia. Images were drawn by Jasmine Chebli.

958

959 Author contributions

960 **JC:** Conceptualization, Formal analysis, Investigation, Visualization, Methodology, Data
961 curation, Project administration, Writing - original draft, Writing - review and editing. **MR,**
962 **TL, AO and BE:** Formal analysis, Writing - review and editing. **HZ:** Resources, Supervision,

963 Funding acquisition, Writing - original draft, Project administration, Writing - review and
964 editing. **AA:** Conceptualization, Supervision, Formal analysis, Investigation, Visualization,
965 Methodology, Writing - original draft, Project administration, Writing - review and editing. All
966 authors reviewed and approved the final manuscript.

967

968 **Author ORCIDs:** JC: 0000-0003-0791-3198, TL: 0000-0001-7389-0348, AO: 0000-0002-
969 5758-7397, HZ: 0000-0003-3930-4354, AA: 0000-0002-4715-9225.

970

971 **Additional information**

972 **Competing interests:** The authors have no competing interests of relevance to the current
973 manuscript.

974 **Funding:** The study was supported by grants from the Swedish Research Council (#2018-
975 02532), the European Research Council (#681712), Stiftelsen för Gamla Tjänarinnor, and
976 Hjärnfonden, Sweden. HZ is a Wallenberg Scholar. TL is funded by an Alzheimer's Research
977 UK senior fellowship. The Queen Square Brain Bank for Neurological Disorders is supported
978 by the Reta Lila Weston Institute for Neurological Studies.

979

980 **Figure legends**

981 **Figure 1. Expression pattern of *appa* and *appb* mRNA.** (A,B) Schematic representations of
982 head and ventricle morphology of a 30 hpf zebrafish larvae, lateral (A) and dorsal (B) view.
983 (C,H) Whole-mount fluorescent *in situ* of *appa* (C) and *appb* (H) in 30 hpf WT zebrafish larvae.
984 Single focal planes, dorsal to ventral, of whole-mount larvae of *appa* (D-G) and *appb* (I-L)
985 probe. (M) Schematic view of focal plane of the dorsal area of the brain ventricle. (N-Q) Single
986 focal plane at high magnification (40x) of *appa* (N,O) and *appb* (P,Q) probes. T= telencephalic
987 ventricle, D/M= diencephalic/mesencephalic ventricle, R= rhombencephalic ventricle, Ob=
988 olfactory bulb, Oe= olfactory epithelium, P= pituitary gland, Le= lens, Ot= optic tectum, Tg=
989 trigeminal ganglia, Rh= rhombomeres, Ov= otic vesicle. Magnification: (C-L)= 20x, (N-Q)=
990 40x. Scale bar: (C)=100μm, (D)= 50μm, (N)= 25μm. * indicates ventricular space and arrows
991 highlight expression.

992

993 **Figure 2. Localization of App protein to cilia of the olfactory sensory neurons and otic**
994 **vesicle in 31 hpf larvae.** Cilia as shown by immunostaining for acetylated tubulin (magenta)
995 and App (green) of the olfactory sensory neurons in the nose epithelium (A) and the otic vesicle
996 (B-C). In (A), dotted lines demarcate the cilia from the nasal cavity (see asterisk). (A') App
997 (green) is found along the cilia and accumulating at their base. Otic vesicle of 24 hpf (B) and
998 31 hpf larvae (C). In (B), glutamylated tubulin (cyan) highlights the base of the cilia outlined
999 by acetylated tubulin staining (magenta). (B) Overview of the kinocilia and stereocilia of the
1000 otic vesicle. The white asterisks indicate accumulation of App (green) at the base of the cilia
1001 bundles. (B') Magnification of cilia outlined in (B). (B'') Increased intensity of the green
1002 channel to detect App (arrows) in kinocilia. Otic vesicle in 31hpf zebrafish larvae (C) with
1003 close-up (C') showing App puncta (green) along the kinocilia. Intensity profiles of acetylated
1004 tubulin (magenta) and App (green) staining from the kinocilia (D-F). In (D), the intensity profile

1005 of the whole length of the kinocilium is plotted whereas profiles of cross-section lines are
1006 plotted with a visible App puncta (**E**) and without (**F**). The dotted lines (**C'**) indicate the
1007 kinocilium and cross-sections. Magnification: (**A-C**)= 40x. Scale bar: (**A**)= 5 μ m, (**B**)= 10 μ m,
1008 (**B'**)= 4 μ m, (**B''**)= 2 μ m, (**C**)= 10 μ m.

1009

1010 **Figure 3.** App localizes to the cilia decorating the ventricle of larvae and ependymal cells in
1011 adult zebrafish. (**A**) Schematic representations of head and ventricle morphology in 30 hpf
1012 zebrafish larvae, dorsal view. (**B**) Dorsal view of ventricle immunostained for App (green) and
1013 acetylated tubulin (magenta) in 30 hpf WT zebrafish larvae. (**C**) Close-up of cilia (magenta)
1014 and App (green). (**D**) Schematic outline of adult zebrafish brain, lateral view. (**E-F**) Coronal
1015 section of adult zebrafish brain and the central canal (see asterisk). Cell nuclei labeled with
1016 DAPI (blue), acetylated tubulin (magenta), App (green). (**F**) Ependymal motile cilia (magenta)
1017 of the central canal with App (green) accumulation along cilia. Magnification: (**B, E**)=10x, (**C,**
1018 **F**)=60x. Scale bar: (**B**)= 50 μ m, (**C**)= 1 μ m, (**E**)= 500 μ m, (**F**)= 10 μ m.

1019

1020 **Figure 4.** APP is localized to the ependymal cilia in adult mouse. (**A**) Schematic representation
1021 of adult mouse brain ventricular system, sagittal view. (**B**) Overview of sagittal section from
1022 adult mouse brain and the third ventricle (see dotted square in (**A**)) for cell nuclei stained with
1023 DAPI (blue), acetylated tubulin (magenta), APP (green). (**C-D**) Close-up of ependymal cells
1024 and their cilia tufts (magenta) and APP expression with anti-APP Y188 antibody (**C**) and 22C11
1025 antibody (**D**). LV= lateral ventricle, III= third ventricle, IV= fourth ventricle, H=hippocampus,
1026 Cp= choroid plexus, Ep= ependyme. Magnification: (**B**)=10x, (**C,D**)=60x. Scale bar: (**B**)=
1027 200 μ m, (**C,D**)= 10 μ m.

1028

1029 **Figure 5.** APP is localized to human ependymal cilia. **(A)** Brightfield overview of a human
1030 brain section of the caudate nucleus immunostained with an anti-acetylated tubulin antibody
1031 reveals the different cellular layers (I-IV): (I) ependyme layer with motile cilia orienting
1032 towards the ventricle lumen, (II) cellular extensions connecting the ependymal cells, (III)
1033 cellular layer dense in astrocytes, (IV) brain parenchyma. **(B-E)** Higher magnifications of the
1034 ependymal layer show clear cilia (acetylated tubulin **(B,D)**) and APP (Y188 antibody **(C,E)**)
1035 accumulation within ependymal cells and along ependymal cilia. **(E')**. Arrows highlight
1036 ependymal cilia tufts in the ventricular lumen. White asterisks indicate broken or absent cilia.
1037 Dotted lines delimitate the ependymal cell layer. Magnification: **(A)**=20x, **(B-C)**= 40x, **(D-E)**=
1038 100x. Scale bar: **(A)**= 5 μ m, **(B)**= 10 μ m, **(D)**= 2 μ m.

1039

1040 **Figure 6.** Generation of *appa*^{-/-} and analysis of *appa*^{-/-}*appb*^{-/-} double mutant zebrafish. **(A)**
1041 Schematic outline of the *appa* gene with exons (black box) and UTR regions (white box).
1042 sgRNA used to target exon 2 with protospacer adjacent motif (PAM) in red and the sgRNA
1043 target sequence underlined. **(B)** Sanger sequencing chromatogram of exon 2 in wild-type and
1044 *appa*^{-/-} zebrafish. **(C)** Schematic drawing of the wild-type Appa protein (738 aa) with epitopes
1045 of antibodies (dotted squares) used above and the hypothetical truncated Appa (109 aa) protein
1046 produced in *appa* mutant below. **(D)** qPCR quantification of *appa* and *appb* mRNA levels in
1047 wild-type and *appa*^{-/-}*appb*^{-/-} mutants at 24 hpf. **(E)** Western blot of 3 dpf whole larvae zebrafish
1048 with antibodies against 22C11 and App (Y188). Alpha-tubulin is used as loading control. Blots
1049 cropped from the same original gel and grouped. Quantification of band intensity are shown
1050 relative to control. Data are reported as mean \pm SD. ** $p < 0.05$, **** $p < 0.001$. qPCR n=5,
1051 WB n=3. SP= signal peptide, E1= extracellular domain, ED= extension domain, AcD= acidic
1052 domain, E2= extracellular domain 2, JMR= juxtamembrane region, A β = amyloid beta, TM=
1053 transmembrane, AICD= amyloid intracellular domain.

1054 **Figure 7.** Longer cilia of dorsal brain ventricle neuroepithelium in *appa^{-/-}appb^{-/-}* larvae
1055 zebrafish. At 30hpf, *appa^{-/-}appb^{-/-}* exhibit longer diencephalic/mesencephalic ventricle cilia
1056 than WT. Data are reported as mean ± SEM. *** $p < 0.001$. n=10 WT (1091 cilia), 16 *appa^{-/-}*
1057 *appb^{-/-}* (1511 cilia).

1058

1059 **Figure 8.** Structural integrity of ependymal cilia in WT and *appa^{-/-}appb^{-/-}* zebrafish.
1060 Transmission electron microscopy of adult zebrafish ependymal cilia of WT (**A-D**) and *appa^{-/-}*
1061 *appb^{-/-}* mutant (**E-H**) adult zebrafish. (**A,E**) Overview of ependymal cilia of the central canal.
1062 (**B,F**) Longitudinal view on the axoneme of the cilia composing its core, the transition zone
1063 including the ciliary pit between the cilia core and the cellular membrane and the basal body
1064 containing the cilia centrioles, highlighted with increased signal. In (**C,G**), cross-sections of
1065 cilia. (**D-H**) Zoom on cross-section of individual cilia showing (9+2) microtubule doublet
1066 organization. Scale bar: (**A,E**)= 1μm, (**B-C, F-G**)= 200 nm, (**D,H**)= 50 nm.

1067

1068 **Figure 9.** The *appa^{-/-}appb^{-/-}* 2 dpf larvae zebrafish exhibit smaller brain ventricle. Dorsal 3D
1069 surface rendering of confocal stacks taken from brain ventricles of dextran injected 2 dpf
1070 zebrafish larvae (**A**). Quantification of total ventricle surface area and volume show that both
1071 are decreased in *appa^{-/-}appb^{-/-}* larvae (**B**). Lateral 3D surface rendering of confocal stacks from
1072 brain ventricles of dextran injected 2 dpf zebrafish larvae with close up on diencephalic
1073 ventricle (**C**). Quantification of surface area and volume of the diencephalic ventricle in WT
1074 and *appa^{-/-}appb^{-/-}* larvae (**D**). Measurement of gross ventricle morphology at 2dpf WT and *appa^{-/-}*
1075 *appb^{-/-}* larvae as the length (**E**). Distance between rostral to caudal, diencephalon ventricle
1076 sagittal length, amplitude and height show no significant difference in mutants (**F**). Data are

1077 reported as mean \pm SEM. ** $p < 0.01$, **** $p < 0.001$. n: (B) WT=19, $appa^{/-}appb^{/-}$ = 34, (D)
1078 WT=8, $appa^{/-}appb^{/-}$ = 34, (F) WT=5, $appa^{/-}appb^{/-}$ = 4.

1079

Supplementary Files

This is a list of supplementary files associated with this preprint. Click to download.

- [SupplementarymaterialsCheblietal.pdf](#)